63-2-3

APGC-TDR-62-74

Solution of Visco-Plastic Equations for Axisymmetric Hypervelocity Impact

Second Summary Report
3 November 1961-2 November 1962

APGC Technical Documentary Report No. APGC-TDR-62-74

DECEMBER 1962 • AFSC Project No. 9860

DEPUTY FOR AEROSPACE SYSTEMS TEST
AIR PROVING GROUND CENTER
AIR FORCE SYSTEMS COMMAND • UNITED STATES AIR FORCE

EGLIN AIR FORCE BASE, FLORIDA

(Prepared under Contract No. AF 08(635)-1713 by Space Sciences Laboratory, General Electric Co., Valley Forge Space Technology Center, King of Prussia, Pa. T. D. Riney, Author)

FOREWORD

This second summary report was prepared by the Space Sciences Laboratory of the General Electric Missile and Space Division, under Air Force Contract No. AF 08(635)-1713, "Theory of High Speed Impact and Theoretical Terminal Ballistics Study". This report together with the first summary report (Reference 6) represent the final report on the contract. The work was administered under the direction of the Ballistics Directorate of the Eglin Air Force Base, with Mr. Andrew Bilek as Project Engineer.

The author wishes to express his appreciation to Dr. Francis H. Harlow of the Los Alamos Laboratories for helpful discussions relative to the numerical scheme and for a copy of his unpublished manuscript. He is pleased to acknowlege the ingenuity and diligence of Dr. J. G. Jewell, Mr. P. J. Usavage and Mr. A. B. Sinopoli of the General Electric Company in developing the actual computer program. Finally, the author wishes to thank Dr. F. W. Wendt for his encouragement and support throughout the investigation.

Catalog cards may be found in the back of this document.

ABSTRACT

The dynamic response of a metallic body when impacted by a hypervelocity projectile is a complicated phenomenon involving the introduction of damage mechanisms which are not completely understood, even when independently operative. In Part I of this report, tentative phenomenological relations are proposed for the hypervelocity impact regime. They include (a) the flow resistance coefficient (which is of fundamental importance in the visco-plastic model for high speed impact), (b) the equation of state for both compressive and rarefaction regions of the metal, and (c) a fracture criterion for high intensity tri-axial stress distributions of extremely short duration.

In Part II of the report a step-by-step description of a computational procedure is presented for the solution of the visco-plastic equations governing the axisymmetric hypervelocity impact situation. The procedure incorporates the above phenomenological relations which are necessary for a realistic description of the penetration and cratering processes. Finally, a brief resume is given of the considerations that were involved in developing PICWICK, an IBM 7090 computer program for carrying out the complex and lengthy computational procedure. This unique program is a basic tool in the development of a more complete theoretical understanding of the hypervelocity impact phenomenon.

PUBLICATION REVIEW

This technical documentary report has been reviewed and is approved.

MORRILL E. MARSTON
Colonel, USAF
Deputy for Aerospace Systems Test

TABLE OF CONTENTS

TABLE OF CONTENTS (Continued)

LIST OF TABLES

LIST OF ILLUSTRATIONS

LIST OF ILLUSTRATIONS (Continued)

LIST OF SYMBOLS

S	yield value of shear stress
S_o	approximate value of S when thermodynamic effects ignored
η	viscosity factor
η_o	approximate value of η when thermodynamic effects ignored
ρ_o	mass density of undisturbed visco-plastic medium
ρ	density of visco-plastic medium
v_o	impact velocity of projectile
D^2	strain-rate invariant
μ	flow-resistance coefficient
D_{ik}	components of strain-rate tensor
τ_{ik}	components of stress tensor
V_{ik}	components of viscous stress tensor
τ^2	Mises flow statistic
t	time
(r, θ, z)	cylindrical coordinates
$\bar{u} = (u, 0, v)$	velocity of flow of medium in Eulerian coordinates
p	thermodynamic pressure
T	absolute temperature
I	specific internal energy
ϵ	parameter used to make μ continuous
c	mean value of specific heat at zero pressure

A, C	material parameters defined by relation (7)
μ_i	material parameters defined by relation (8)
r_i	material parameters defined by relation (14)
σ_{cr}	critical fracture parameter
U_o, γ, t_o	material parameters defined by relation (22)
λ, ω, t_o	material parameters defined by relation (24)
δt	size of time mesh
h	size of space mesh in radial direction
k	size of space mesh in axial direction
s	length of sides of space mesh when $h = k (= s)$
e	sum of specific kinetic and internal energies
N	number of mass particles originally in each cell
$H = 2dh$	diameter of projectile
$L = \ell k$	length of projectile
β	number of columns in space mesh
γ	number of rows in space mesh
P, Q	functions defined by relation (A-6)
Λ, Ω	functions defined by relations (40) and (41)
Ψ, Γ	functions defined by relations (38) and (39)
M	total mass of particles in cell
(m_ν, r_ν, z_ν)	mass and coordinates of ν-th particle
R	total radial momentum in cell

Z	total axial momentum in cell
E	total energy in cell
$(\tilde{\ })$	result of Phase I calculation for ( )
$(\ )$	result of Phase II calculation for ( )
$(\hat{\ })$	value of ( ) computed using mean values of the velocities
$(\ )_i^j$	cell wise value of quantity in cell $\binom{j}{i}$

INTRODUCTION

The dynamic response of a metallic body in impact by a hypervelocity projectile is a complicated phenomenon involving the introduction of damage mechanisms which are not completely understood even when independently operative. However, a qualitative model of crater formation has evolved, based on experimental investigations of impact at velocities as high as 2 cm/μ sec.* Tests in which the actual cratering process has been monitored by high speed photography and flash X-ray photography have shown that the crater may continue to enlarge for several hundred microseconds even though only five to ten microseconds are required to use up the projectile (Reference 1). The mechanism of crater formation is therefore essentially one of cavitation, the size and shape of the final crater being determined by the pressure wave established during the first five to ten microseconds by the action of the projectile on the target, and by the resistance of the target material to flow. The flow continues until the amplitude of the wave decreases below the intrinsic yield strength of the target material.

In previous reports (References 2 through 4) the available experimental data have been studied and a visco-plastic model has been formulated which takes into account the above characteristic effects. This model includes the viscous and strength effects of the impacted metals as well as the inertial effect. The importance of including all three effects in the model was demonstrated quantitatively by numerical solution of the system of equations governing the model in the case of a one-dimensional impact situation. The results of these earlier investigations were discussed in detail in References 5 and 6.

The object of this phase of the theoretical investigation of the hypervelocity impact phenomenon is the solution of the governing equations for the axisymmetric case depicted in Figure 1. This configuration requires the solution of the system of two-dimensional, time dependent partial differential equations given in Appendix A; a large difference exists in the difficulty between the 1-D and 2-D problems.

*The gram-centimeter microsecond system of units is used throughout this report. The unit of stress becomes the megabar (mb).

In developing a finite difference formulation of the axisymmetic impact problem it is natural to attempt an extension of an existing scheme devised for two-dimensional hydrodynamics; this has been our approach (References 7 and 8). In addition to the obvious difficulties of extending the computational procedure to the much more complicated system of equations governing the visco-plastic model, the description of the axisymmetric impact problem must also include provisions for negative pressure and material fracture (Reference 9). The fundamental importance of these phenomena in the cratering process is depicted by the sequence of illustrations in Figure 2. The rupture of the material and its ejection from the crater during the cavitation process accounts for a large percentage of the final crater volume. In Part I of this report phenomenological relations are proposed which permit these phenomena to be included in the theoretical model.

Part II of this report gives a comprehensive summary of the various considerations that have gone into the development of a numerical scheme for the solution of the axisymmetric hypervelocity impact problem. The description is complete enough that a programmer may work directly from this report. Indeed a computer code for the IBM 7090 (or 7094) has been completed and is in operation. The program is named PICWICK; its salient features are described in the final section of this report.

PART I: PHENOMENOLOGICAL RELATIONS

For each material requiring calculations the equation of state, the flow-resistance coefficient, and the fracture criteria for a dynamic tri-axial stress condition must be specified. Actually, none of these have been firmly established by experiments under the severe conditions of pressure, strain-rate, and temperature which occur during hypervelocity impact. At the present state of knowledge it is necessary to extrapolate boldly from data observed under far less severe conditions. This is not so important from the theoretical viewpoint as the ability of the analysis to include and compare various proposed constitutive relations. To facilitate the evaluation of these various hypotheses, the equation of state, the flow-resistance coefficient, and the fracture criterion have been written into the program as sub-routines so that they may be readily changed.

In this part of the report tentative constitutive relations are proposed for the hypervelocity regime. As more experimental data become available, and as computational experiments are performed, improved hypotheses are expected to evolve.

FLOW-RESISTANCE COEFFICIENT

The response of the projectile and target materials when subjected to hypervelocity impact is governed by the system of visco-plastic equations formulated earlier in this study (References 2 and 6). The equations were constructed to bridge the transistion from the plastic to the hydrodynamic regimes in the simplest manner consistent with the physical requirement that the inertial (compressibility), viscous, and strength effects be included.

Thus the stress tensor τ_{ik} and the strain-rate tensor, D_{ik}, were assumed related acording to

$$\tau_{ik} = - p\delta_{ik} + \mu D_{ik} - \frac{2}{3} \mu \operatorname{div} \bar{u}\, \delta_{ik}; \qquad (1)$$

the essential new feature of the model was the introduction of the flow-resistance coefficient

$$\mu(D) = \eta_o + \frac{S_o}{\sqrt{D^2}} \qquad (|\tau| \geq S_o)$$

$$= \infty \qquad (|\tau| < S_o)$$

into the usual momentum and energy equations of continuum mechanics. The quantity D^2 denotes the second invariant of the deformation strain-rate tensor, S_o denotes the static yield shear stress of the material, η_o denotes the viscosity factor, and $\tau^2 = \mu^2 D^2$ is a measure of the deformation experienced by the medium. Thus, the material was considered rigid if stressed below its yield strength, whereas above this value it was assumed to behave as a Newtonian viscous liquid.

Recently (Reference 8), a small parameter $\epsilon > 0$ was incorporated into the definition of the flow resistance coefficient,

$$\mu(D) = \eta_o + \frac{S_o}{\sqrt{D^2 + \epsilon}} \cdot \qquad (2)$$

It was introduced chiefly to remove the moving surface of separation between the rigid and fluid regions of the medium. This not only simplifies the calculations, however, but is also more realistic because the shearing stresses now depend upon the strain-rate in a continuous manner. Under prolonged loading this model permits deformation to occur even for $|\tau| < S_o$, but the impact mechanism is completed long before such creep effects can occur.

Actually both η_o and S_o are not constant but depend on the thermodynamic state of the medium:

$$\eta_o \rightarrow \eta(I, p) \qquad S_o \rightarrow S(I, p) .$$

Both decrease in value if the specific internal energy (essentially the temperature) is increased while holding the pressure constant,

$$\left(\frac{\partial \eta}{\partial I}\right)_{p_o} < 0 \qquad \left(\frac{\partial S}{\partial I}\right)_{p_o} < 0 ; \qquad (3)$$

both increase in value if the pressure is increased while the internal energy is held constant,

$$\left(\frac{\partial \eta}{\partial p}\right)_{I_o} > 0 \qquad \left(\frac{\partial S}{\partial p}\right)_{I_o} > 0 . \tag{4}$$

In order to explicitly account for these effects, the definition of the flow-resistance coefficients will be written as follows: *

$$\mu \equiv \mu(I, p, D)$$

$$\equiv \eta(I, p) + \frac{S(I, p)}{\sqrt{D^2 + \epsilon}} . \tag{5}$$

The internal energy, pressure, and strain-rate dependence of μ are depicted schematically in Figure 3. The governing equations are given in Appendix A.

To appreciate the significance of the dependence of μ on the thermodynamic variables, substitute the continuity equation into the adiabatic energy equation to obtain

$$\frac{dI}{dt} = \rho^{-1}\left[\mu D^2 + p\rho^{-1}\frac{d\rho}{dt}\right]; \tag{6}$$

the specific internal energy therefore increases monotonically with increasing strain-rate (compressive). In view of (3) and (5) it follows that, for a given final compression, the flow-resistance coefficient of the medium will decrease rapidly with an increase in the strain-rate. The decrease in the flow-resistance, in turn, permits a further increase in the strain-rate. The decreased resistance to deformation at extreme strain-rates has been observed to be extremely important in the cratering process, as it permits the cavitation flow to continue a long time after impact (Reference 1). Since the greater part of the crater is formed during the cavitation flow, the dependence of η and S on the thermodynamic state of the medium cannot be safely neglected.

This feedback between the temperature and further decrease in flow-resistance is currently the subject of research by Dr. I. J. Gruntfest (Reference 10).

---

*The flow-resistance coefficient is not restricted to the form in relation (5). The numerical method can treat any general function $\mu = \mu(I, p, D)$.

SURVEY OF FLOW-RESISTANCE DATA

There are apparently no measurements of the flow-resistance coefficients of materials under the conditions of temperature, pressure, and strain-rate that occur in hypervelocity impact. Data are available, however, in the following isolated thermodynamic ranges:

a. Viscosity measurements of molten metals at atmospheric pressure.

b. Longtime, low-load creep.

c. Plastic wave propagation in metal bars.

d. Static yield stress measurements as functions of pressure and temperature.

These data have been surveyed to give rough estimates for the functions $\eta(I, p)$ and $S(I, p)$.

a) Molten Metals

Above its melting temperature the yield strength of a metal vanishes, $S = 0$, and the flow-resistance coefficient reduces to the ordinary viscosity factor, $\mu = \eta$. Experimental values of μ are therefore available in the elevated temperature range (at atmospheric pressure) from measurements of the flow-resistance of the liquid phase. The experimental results for a number of metals are presented in Figure 4. The viscosity factor is seen to vary with the absolute temperature according to the relation

$$[\eta]_{p=0} = A \exp(C/T) . \tag{7}$$

The values of A and C are given in Table I for the various metals.

It has been observed that the flow-resistance of a metal suddenly increases as the temperature is lowered to its melting point (Reference 14). According to the present hypothesis, equation (5), this effect may be assumed to be a consequence of S assuming a non-zero value at the freezing temperature rather than indicating a discontinuity in η. With this interpretation, the above exponential relation may be used to make zero-order estimates for the solid phase values of η.

The specific internal energy will be set equal to zero when T = 300°K and p = 0. Then equation (7) is essentially equivalent to

$$\eta(I, 0) = \mu_o \exp\left(\frac{\mu_1}{I + \mu_2}\right), \tag{8}$$

where $\mu_o = A$, $\mu_1 = cC$, $\mu_2 = 300c$ and c is a mean value of the specific heat at zero pressure. The values of μ_o, μ_1, and μ_2 are listed in Table I, as are the estimated values of

$$\eta(0, 0) = \mu_o \exp(\mu_1/\mu_2).$$

b) Creep Data

Creep data is ordinarily generated by studying the long-term elongation of a long rod subjected to uniaxial tension (along z-axis). Then

$$\tau_{rr} = \tau_{\theta\theta} = 0 \qquad p = -\frac{1}{3}\tau_{zz}$$

$$D_{rz} = 0 \qquad D_{rr} = D_{\theta\theta} = -\frac{1}{2}D_{zz} \qquad \operatorname{div} \bar{u} \approx 0.$$

The flow-resistance coefficient and the axial stress reduce to

$$\mu = \eta\left(I, -\frac{1}{3}\tau_{zz}\right) + \frac{S\left(I, -\frac{1}{3}\tau_{zz}\right)}{\sqrt{3}\frac{\partial v}{\partial z} + \epsilon} \tag{9}$$

$$\tau_{zz} = 3\mu\frac{\partial v}{\partial z}. \tag{10}$$

In this range therefore, μ will be very large since ϵ and $\partial v/\partial z$ are small.

For example, in the case of high-purity polycrystalline aluminum subjected to long term creep (Reference 15):

$$T = 478^{\circ}K (I = 1.71 \times 10^{-3}),\ \tau_{zz} = 2.1 \times 10^{-4},\ \frac{\partial v}{\partial z} = 10^{-11},$$

$$S = 2 \times 10^{-4}.\ *$$

Hence, using (10),

$$\mu \approx \frac{2.1 \times 10^{-4}}{3 \times 10^{-11}} = 0.7 \times 10^{7}.$$

The first term on the right side of (9) is approximated by 6×10^{-11}. It is therefore negligible and we may write $0.7 \times 10^{7} \approx 2 \times 10^{-4}\ \epsilon$, whence,

$$\text{Aluminum:}\quad \epsilon \approx 3 \times 10^{-11}$$

Actually, the true value of ϵ is unimportant in impact calculations. It will therefore be assigned as convenient in the calculations without regard to values estimated from creep data. It must, however, be kept small.

c) Plastic Wave Propagation

Dynamic stress-strain curves for high-purity, polycrystalline aluminum have recently been presented by Hauser, Simmons, and Dorn (Reference 16). For static tests made at $T_o = 295^{\circ}K$ the yield stress was $\sqrt{3}\ S_o \approx 0.77 \times 10^{-3}$. The dynamic stress at a total strain of 16% was observed to be 1.96×10^{-3} and 1.36×10^{-3} for strain rates of 10^{-2} and 10^{-3} respectively. Equations (9) and (10) may again be used to estimate η since div $\bar{u} \approx 0$ in these tests:

$$\tau_{zz} = 3\left(\eta_o + \frac{S_o}{\sqrt{3}\ \frac{\partial v}{\partial z} + \epsilon}\right)\frac{\partial v}{\partial z} \approx 3\eta_o \frac{\partial v}{\partial z} + \sqrt{3}\ S_o$$

*The gram-centimeter-microsecond system of units is used throughout this report.

or

$$\eta_o = \frac{\tau_{zz} - \sqrt{3}\, S_o}{\sqrt{3}\, \frac{\partial v}{\partial z}}$$

$$\text{Aluminum:} \quad \begin{cases} \eta_o = 0.04 & \text{for strain-rate of } 10^{-2} \\ \eta_o = 0.20 & \text{for strain-rate of } 10^{-3} \,. \end{cases} \tag{11}$$

These results simply verify that the viscosity factor cannot be regarded as constant. The decrease in its value with increase in the strain-rate may be assigned to the greater specific internal energy of the medium. If the strain-rate 10^{-2} is great enough for a truly adiabatic situation, the increase in specific internal energy is roughly estimated by

$$\Delta I \approx \frac{1}{2}\, t^* \left(\frac{dI}{dt}\right)_{t^*} , \tag{12}$$

where t^* = time duration of test = $0.16/10^{-2}$ = 16 μsec. and (6) may be used to approximate dI/dt. This procedure yields an estimate of $\Delta I \approx 7.5 \times 10^{-5}$ which corresponds to a temperature rise of $\Delta T \approx 8.5^{\circ}K$. If we assume that in this regime the temperature dependence of η is also of the form $A \exp(C/T)$ the estimates for the parameters would be $A = 0.113$ and $C = 170$ as opposed to the values $A = 10^{-11}$ and $C = 7580$ deduced from the molten metal data. The former values may be regarded as a first order approximation.

The values of η_o listed in (11) compare favorably with the value of 0.23 assumed by Malvern (Reference 17) in his original study of the strain-rate effect in aluminum rods. Values for steel and copper have been estimated by Perzyna (Reference 18):

$$\begin{aligned} &\text{Iron:} && \eta_o = 0.8 \text{ gm. cm}^{-1} \mu\text{sec}^{-1} \text{ (Perzyna)} \\ &\text{Copper:} && \eta_o = 0.4 \text{ gm. cm}^{-1} \mu\text{sec}^{-1} \text{ (Perzyna)} \\ &\text{Aluminum:} && \eta_o = 0.23 \text{ gm. cm}^{-1} \mu\text{sec}^{-1} \text{ (Malvern).} \end{aligned} \tag{13}$$

d) Thermodynamic Dependence of Yield Strength

The literature contains sufficient data relating to the temperature dependence of the yield strength of metals under atmospheric pressure conditions (e. g., Reference 19). The function

$$S(I, 0) = r_o \exp\left(\frac{r_1}{I + r_2}\right) \tag{14}$$

may be fitted to the data for any particular metal. No special significance is attached to the form; it merely has the property of decreasing with an increase in I and contains a sufficient number of material parameters to permit the required flexibility.

As a result of static tension tests under hydrostatic pressure Bridgeman concludes (Reference 20, p 70) that the yield stress is raised by an amount roughly proportional to the pressure. The combined effects of pressure and temperature have apparently not been investigated even under static conditions.

EQUATION OF STATE

In the compressive regime the most reliable equation of state available has been determined by the Los Alamos group from velocity measurements of shock waves induced by high explosives. The pressure is expressed as a function of density and specific internal energy (Reference 21).

$$p = f(\rho, I)$$

where

$$\begin{aligned} f(\rho, I) = \frac{1}{\phi + \phi_o}\Big[&(a_1 + a_2\,\zeta)\,\zeta\,(1 - \xi_2\,\lambda^2) \\ &+ \phi\,\Big\{\Big[b_o + (b_1 + b_2\,\zeta)\,\zeta\Big]\Big[1 + \xi_2\,\lambda\,(1 - \lambda)\Big] \\ &+ \phi\,(c_o + c_1\,\zeta)\,\Big[1 - \xi_2(1 - \lambda)^2\Big]\Big\} - \xi_1\,(\zeta + 1)^2\,(a_2 + b_2\,\phi)\Big]\,. \end{aligned} \tag{15}$$

Here, there are introduced the notations

$$\zeta = \frac{\rho}{\rho_o} - 1 \qquad \phi = \rho_o I \qquad \lambda = \frac{\phi}{\phi + \phi_o} \tag{16}$$

and the material parameters

$$a_1,\ a_2,\ b_o,\ b_1,\ b_2,\ c_o,\ c_1,\ \phi_o,\ \xi_1,\ \xi_2. \tag{17}$$

The specific internal energy in the undisturbed material is zero, $I_o = 0$. Throughout the calculations $I \geq 0$.

It is also necessary to provide an equation of state for the tensile regime since rarefaction regions occur near the edge of the projectile-target interface during the early stages of the process, and near the lip of the forming crater during the later stages. Apparently no experimental data are available under these extreme conditions. It seems reasonable and expedient to use the tangent line of $f(\rho, I)$ to extend the equation of state into the tensile regime (Figure 5):

$$h(\rho, I) = \zeta \left[\frac{\partial f}{\partial \zeta}\right]_{\zeta = 0} + [f]_{\zeta = 0}$$

or

$$h(\rho, I) = \frac{1}{\phi + \phi_0}\left[a_1 \zeta (1 - \xi_2 \lambda^2) + \phi \left\{\left[b_o + b_1 \zeta\right]\left[1 + \xi_2 \lambda (1 - \lambda)\right] + \phi (c_o + c_1 \zeta)\left[1 - \xi_2 (1 - \lambda)^2\right]\right\} - \xi_1 (2\zeta + 1)(a_2 + b_2 \phi)\right] \tag{18}$$

The equation of state is therefore assumed to be given by the following composite formula:

$$p = F(\rho, I)$$

where

$$F(\rho, I) = f(\rho, I) \quad \text{if } \zeta \geq 0$$
$$= h(\rho, I) \quad \text{if } \zeta < 0 \,. \tag{19}$$

The material parameters (17) are listed in Table II for aluminum and iron. Values are also available for most other metals of interest but they are apparently still classified.

FRACTURE CRITERION

To account for the ejection of material from the lip of the crater during formation, it is necessary to incorporate a dynamic fracture criterion into the calculations. If no such provision is made, one would be tacitly assuming extremely large fracture strengths for the projectile-target materials. The consequence would be that no material would be ejected from the target (which would be contrary to experimental observations) and the calculated crater dimensions would be much smaller than are actually found.

The material is subjected to tri-axial stress under extreme conditions of temperature and strain-rate. No fracture criterion has been established under these conditions. In the present formulation it is assumed that fracture occurs whenever both the pressure is negative (i. e., hydrostatic tension exists) and the maximum deviatoric stress exceeds a critical value:

$$p < 0 \qquad \text{and} \qquad V_{max} \geq \sigma_{cr} \,, \tag{20}$$

where the deviatoric stress components are defined in equation (A-11) and

$$V_{max} = \max \left[\left| V_{rr} \right|, \left| V_{\theta\theta} \right|, \left| V_{zz} \right| \right] \,. \tag{21}$$

The critical value of σ_{cr} will depend upon the temperature and the length of time during which the stress is applied.

A rational assumption is that the damage suffered by a segment of the medium is cumulative; that is, in each small time increment the fracture will proceed at a rate appropriate to the stress distribution and temperature

occurring during that time increment. In the present numerical scheme, however, the stress field is expressed in Eulerian coordinates, and it would be extremely difficult to account for the cumulative damage suffered by the material particles. It is therefore assumed that damage is cumulated only for the time interval, δt, corresponding to one time cycle of the numerical scheme.

In the case of uniaxial loading the fracture criterion most generally accepted for dynamic conditions takes the form (Reference 22):

$$\int_{t_1}^{t_2} \exp\left[-\frac{U_o - \gamma\sigma}{RT}\right] dt = t_o , \tag{22}$$

where R is the gas constant, t_1 is the time in which the stress becomes tensile, t_2 is the time at which fracture occurs, and t_o, U_o, and γ are material constants. To extend this relation in accordance with the above discussion, replace σ by the critical value of V_{max}, σ_{cr}, and cumulate only for time δt to get

$$\exp\left[-\frac{\lambda - \omega\sigma_{cr}}{T}\right] = \frac{t_o}{\delta t} \qquad \lambda = \frac{U_o}{R}, \qquad \omega = \frac{\gamma}{R}$$

or, taking the natural logarithm of both sides and rearranging terms,

$$\sigma_{cr} = \frac{1}{\omega}\left[\lambda - T\,\ell n(\delta t/t_o)\right] . \tag{23}$$

In terms of the specific internal energy, the relation is approximated by

$$\sigma_{cr} = \frac{1}{\omega}\left[\lambda - \left(\frac{I}{c} - 300\right)\ell n\,\frac{\delta t}{t_o}\right] , \tag{24}$$

where c is a mean value of the specific heat.

From experimental results over a wide range of stresses and temperatures Zhurkov (Reference 22, 23, 24) has deduced empirical values for the constants t_o, U_o, and γ for a number of metals. U_o was found to be nearly

equal to the sublimation energy while t_o was found to be of the order of magnitude of the vibration period of the crystal lattice. Zhurkov's results for platinum and aluminum have been replotted in the gram-centimeter-microsecond system of units and are given in Figures 6 and 7 respectively. The approximate values of t_o, λ and ω obtained from these plots are presented in Table III along with estimated values for several other metals.

PART II: METHOD OF SOLUTION

In developing a finite difference formulation of the equations governing the axisymmetric impact problem (Appendix A), the extension of an existing scheme devised for two-dimensional hydrodynamics is a natural approach. Several methods of treatment have been used for those problems dependent upon two or more space coordinates. These variations usually employ (a) Lagrangian coordinates in which the mesh of cells is imbedded in the medium and moves with it (References 29 through 32), (b) Eulerian coordinates which are not fixed in the medium but are usually stationary in the laboratory frame of reference, or (c) a mixed Euler-Lagrange system which attempts to take advantage of the better features of both fixed and moveable coordinates (References 33 through 36).

The chief difficulty with schemes employing Lagrangian coordinates is the large distortion which is involved in the present problem. The Eulerian systems have the disadvantage that to account for the projectile-target interface and the free surfaces of the projectile and target is extremely difficult. These are the basic reasons for the decision to adopt the particle-in-cell method (abbreviated PIC) which has been developed at Los Alamos by Dr. Francis H. Harlow and his colleagues.

In devising the present formulation the basic references have been the series of Los Alamos reports which describe the PIC method (References 33 through 35). An attempt has been made to derive maximum benefit from the experiences of the Los Alamos group in applying the method and to extrapolate their results and heuristic concepts to the more complex problem at hand. This is especially desirable in using the PIC method as it is still an experimental procedure which does not have a firm mathematical basis. The author has had the benefit of extremely fruitful discussions with Dr. Harlow at Los Alamos.

A brief description of the essential features of the method may be given. The space occupied by the medium is divided into a suitably chosen mesh of fixed cells through which the medium moves; the medium within each cell is represented by a set of mass points (particles). At the end of the n-th time cycle the mass (equal to the sum of the masses of the particles located in that cell) velocity, pressure, and specific internal energy are associated with each cell. To obtain the corresponding data at the end of the (n + 1) th time cycle one makes a three phase calculation. In Phase I the field functions are changed neglecting the motion of the medium. In Phase II the mass points are moved and the field functions then recalculated to account for the motion. In Phase III various functionals are computed which furnish checks on the accuracy of the calculations.

FORMULATION OF PROBLEM

The projectile is considered to be a circular cylinder of length L and diameter H. An axial section of the projectile - target configuration at the instant of impact (t = 0) is shown in Figure 8; it is superposed by the fixed space mesh used to describe the subsequent motion of the configuration. On this plane of symmetry the cells of the space mesh appear as rectangles with sides of length $\delta r = h$ by $\delta z = k$; each cell is actually a toroid of revolution. For example, the projectile is initially divided into ℓ x d cells,

$$\ell = L/k \qquad\qquad d = H/2h. \tag{25}$$

The cells are labelled with index $\binom{j}{i}$, with i and j increasing in the r and z directions, respectively:

$$\text{cell}\binom{j}{i} = \begin{cases} (j-1)k \leqq z < j\ k \\ (i-1)h \leqq r < i\ h \end{cases} \quad \begin{matrix} j = 1,\ 2,\ \ldots,\ \gamma \\ i = 1,\ 2,\ \ldots,\ \beta\ . \end{matrix} \tag{26}$$

Thus, each cell includes its left and top boundaries but does not include its right and bottom boundaries.

The projectile-target material is represented in the axial plane by discrete mass points called "particles"; each particle is actually a circle about the axis of symmetry. Having a different mass for different mass particles is convenient in cylindrical coordinates. Each particle is assigned a fixed mass whose value is proportional to the radius of the cell within which it lies originally; i.e., at t = 0. The r and z coordinates of each particle are stored in the computing-machine memory. These are changed in time in accordance with the subsequent motion of the material through the mesh of computational cells.

If there are originally N particles in each cell, then the mass of each of the N particles in cell $\binom{j}{i}$ is

$$\frac{2\pi r_i\, h\, k\, \rho_o}{N} = \frac{2\pi (i - 1/2)\, h^2\, k\, \rho_o}{N}, \quad r_i = (i - 1/2)\, h. \tag{27}$$

The N mass particles are assumed to be originally randomly distributed within each cell. The location of each particle at the end of the n-th time cycle is

stored in the machine memory until its location at the end of the (n + 1)th cycle is computed. The conservation of mass is therefore automatic in the PIC method.

Such dependent variables as velocity, pressure, and specific internal energy are kept in the machine memory by cell. For example, the pressure of cell $\binom{j}{i}$ is denoted by p_i^j; and is meant to represent an average of the pressure throughout the volume of the medium inside the cell at that time. The average pressure along the boundary between cells $\binom{j}{i}$ and $\binom{j-1}{i}$ is denoted by $p_i^{j-1/2}$; while the average pressure between cells $\binom{j}{i}$ and $\binom{j}{i-1}$ is $p_{i-1/2}^j$. Analogous notations are used for the other cell-wise quantities.

DIFFERENCE EQUATIONS

The velocity components and the specific internal energy are advanced in time according to a finite difference approximation of the equations governing the visco-plastic model. This advance occurs during Phase I of the calculations in which the particles are not moved; thus, the transport terms are dropped from the differential equations. The tentative new cellwise velocity components become (see equations A-2 and A-3 in Appendix A):

$$\tilde{u}_i^j = u_i^j + \frac{2\pi(i-1/2)h\,k\,\delta t}{M_i^j}\left\{ P_{i+1/2}^j - P_{i-1/2}^j + \frac{2}{h}\left[\mu_{i+1/2}^j (u_{i+1}^j - u_i^j) - \mu_{i-1/2}^j (u_i^j - u_{i-1}^j) \right] \right\}$$
$$+ \mu_i^j \frac{4\pi(i-1/2)h\,k\,\delta t}{M_i^j} \left\{ \left(\frac{u}{r}\right)_{i+1/2}^j - \left(\frac{u}{r}\right)_{i-1/2}^j \right\} \qquad (28)$$
$$+ \frac{2\pi(i-1/2)h^2\,\delta t}{M_i^j} \left\{ Q_i^{j+1/2} - Q_i^{j-1/2} \right\}$$

$$\tilde{v}_i^j = v_i^j + \frac{2\pi(i-1/2)h^2\,\delta t}{M_i^j}\left\{P_i^{j+1/2} - P_i^{j-1/2} + \frac{2}{k}\left[\mu_i^{j+1/2}(v_i^{j+1} - v_i^j) - \mu_i^{j-1/2}(v_i^j - v_i^{j-1})\right]\right\} + \frac{2\pi k\,\delta t}{M_i^j}\left\{(rQ)_{i+1/2}^j - (rQ)_{i-1/2}^j\right\} \tag{29}$$

where

$$(\operatorname{div}\bar{u})_i^j = \frac{u_{i+1/2}^j - u_{i-1/2}^j}{h} + \frac{u_i^j}{(i-1/2)h} + \frac{v_i^{j+1/2} - v_i^{j-1/2}}{k} \tag{30}$$

$$(D^2)_i^j = \left[\frac{u_i^{j+1/2} - u_i^{j-1/2}}{k} + \frac{v_{i+1/2}^j - v_{i-1/2}^j}{h}\right]^2 + 2\left\{\left[\frac{u_{i+1/2}^j - u_{i-1/2}^j}{h}\right]^2 + \left[\frac{u_i^j}{(i-1/2)h}\right]^2 + \left[\frac{v_i^{j+1/2} - v_i^{j-1/2}}{k}\right]^2\right\} - \frac{2}{3}\left[(\operatorname{div}\bar{u})_i^j\right]^2 \tag{31}$$

$$\mu_i^j = \eta(I_i^j,\ p_i^j) + \frac{S(I_i^j,\ p_i^j)}{\sqrt{(D^2)_i^j} + \epsilon} \tag{32}$$

$$P_i^j = -p_i^j - \frac{2}{3}\mu_i^j(\operatorname{div}\bar{u})_i^j \tag{33}$$

$$Q_i^j = \mu_i^j \left\{ \frac{u_i^{j+1/2} - u_i^{j-1/2}}{k} + \frac{v_{i+1/2}^j - v_{i-1/2}^j}{h} \right\} \tag{34}$$

$$(r^2)_i^j = (D^2)_i^j (\mu_i^j)^2. \tag{35}$$

In computing the tentative new cellwise specific internal energy both $(u_i^j,\ v_i^j)$ and $(\tilde{u}_i^j,\ \tilde{v}_i^j)$ are assumed available in the machine memory. Then with

$$\hat{u} = \frac{1}{2}(u + \tilde{u}) \qquad \hat{v} = \frac{1}{2}(v + \tilde{v}) \tag{36}$$

the proper form is (see equation A-10 of Appendix A)

$$\begin{aligned} \tilde{\Gamma}_i^j = \Gamma_i^j + \frac{2\pi(i-1/2)h^2 k\,\delta t}{M_i^j} \Bigg\{ \frac{1}{h} \Bigg(& \Lambda_{i+1/2}^j - \Lambda_{i-1/2}^j \\ & - \hat{u}_i^j \left[(V_{rr})_{i+1/2}^j - (V_{rr})_{i-1/2}^j \right] - \hat{v}_i^j \left[(V_{rz})_{i+1/2}^j - (V_{rz})_{i-1/2}^j \right] \Bigg) \\ & + \frac{1}{k} \Bigg(\Omega_i^{j+1/2} - \Omega_i^{j-1/2} - \hat{u}_i^j \left[(V_{rz})_i^{j+1/2} - (V_{rz})_i^{j-1/2} \right] \\ & - \hat{v}_i^j \left[(V_{zz})_i^{j+1/2} - (V_{zz})_i^{j-1/2} \right] \Bigg) \Bigg\} \end{aligned} \tag{37}$$

where we have introduced the notations

$$\Gamma_i^j = \Psi_i^j + \frac{2\pi h k\,\delta t}{M_i^j} \hat{u}_i^j (V_{\theta\theta})_i^j \tag{38}$$

$$\Psi_i^j = I_i^j - \frac{2\pi(i-1/2)h^2 k\,\delta t}{M_i^j} p_i^j (\operatorname{div} \overset{\Delta}{u})_i^j \tag{39}$$

$$\Lambda_{i-1/2}^{j} = \frac{1}{2}\left[\hat{u}_{i-1}^{j}(V_{rr})_{i-1}^{j} + \hat{u}_{i}^{j}(V_{rr})_{i}^{j} + \hat{v}_{i-1}^{j}(V_{rz})_{i-1}^{j} + \hat{v}_{i}^{j}(V_{rz})_{i}^{j}\right] \tag{40}$$

$$\Omega_{i}^{j-1/2} = \frac{1}{2}\left[\hat{u}_{i}^{j-1}(V_{rz})_{i}^{j-1} + \hat{u}_{i}^{j}(V_{rz})_{i}^{j} + \hat{v}_{i}^{j-1}(V_{zz})_{i}^{j-1} + \hat{v}_{i}^{j}(V_{zz})_{i}^{j}\right] . \tag{41}$$

The viscous stress components are approximated by the following relations (see equations A-11 of Appendix A):

$$(V_{rr})_{i}^{j} = \hat{\mu}_{i}^{j}\left[\frac{2}{h}(\hat{u}_{i+1/2}^{j} - \hat{u}_{i-1/2}^{j}) - \frac{2}{3}(\operatorname{div}\hat{\underline{u}})_{i}^{j}\right] \tag{42}$$

$$(V_{\theta\theta})_{i}^{j} = \hat{\mu}_{i}^{j}\left[\frac{2}{(i-1/2)h}\hat{u}_{i}^{j} - \frac{2}{3}(\operatorname{div}\hat{\underline{u}})_{i}^{j}\right] \tag{43}$$

$$(V_{zz})_{i}^{j} = \hat{\mu}_{i}^{j}\left[\frac{2}{k}(\hat{v}_{i}^{j+1/2} - \hat{v}_{i}^{j-1/2}) - \frac{2}{3}(\operatorname{div}\hat{\underline{u}})_{i}^{j}\right] \tag{44}$$

$$(V_{rz})_{i}^{j} = \hat{\mu}_{i}^{j}\left[\frac{1}{k}(\hat{u}_{i}^{j+1/2} - \hat{u}_{i}^{j-1/2}) + \frac{1}{h}(\hat{v}_{i+1/2}^{j} - \hat{v}_{i-1/2}^{j})\right] \tag{45}$$

wherein

$$(\operatorname{div}\hat{\underline{u}})_{i}^{j} = \frac{\hat{u}_{i+1/2}^{j} - \hat{u}_{i-1/2}^{j}}{h} + \frac{\hat{u}_{i}^{j}}{(i-1/2)h} + \frac{\hat{v}_{i}^{j+1/2} - \hat{v}_{i}^{j-1/2}}{k} \tag{46}$$

$$(\hat{D}^2)_i^j = \left[\frac{\hat{u}_i^{j+1/2} - \hat{u}_i^{j-1/2}}{k} + \frac{\hat{v}_{i+1/2}^j - \hat{v}_{i-1/2}^j}{h}\right]^2$$

$$+ 2\left\{\left[\frac{\hat{u}_{i+1/2}^j - \hat{u}_{i-1/2}^j}{h}\right]^2 + \left[\frac{\hat{u}_i^j}{(i-1/2)h}\right]^2 \right. \tag{47}$$

$$\left. + \left[\frac{\hat{v}_i^{j+1/2} - \hat{v}_i^{j-1/2}}{k}\right]^2\right\} - \frac{2}{3}\left[(\operatorname{div} \hat{\underline{u}})_i^j\right]^2$$

$$\hat{\mu}_i^j = \eta(I_i^j,\ p_i^j) + \frac{S(I_i^j,\ p_i^j)}{\sqrt{(\hat{D}^2)_i^j} + \epsilon} \quad . \tag{48}$$

PHASE I - CALCULATIONS

No mass particles are permitted to cross the left boundary of the mesh (axis of symmetry) as this would violate the assumption of rotational symmetry. No such restriction applies at the top, bottom and right boundaries of the mesh; these are treated as "continuative boundaries". Accordingly, the boundary cells along these three sides are treated as interior, being bounded on the outside by cells with identically the same properties at any instant as their adjacent interior neighbors.

Special considerations are also required when computing in a cell adjacent to an empty cell (if the cell itself is empty no calculations are made). The velocity of the empty cell is then assumed to be equal to that of the cell being computed; the pressure and the viscosity stresses are assumed to vanish on the boundary of an empty cell. In the following step-by-step description of the computational procedure these special considerations are treated in detail (a programmer may work directly from this report).

At the end of the n - th cycle, the mass, specific internal energy, velocity components, and the pressure for every cell are stored in the memory. Table IV shows these together with the quantities which replace them during the sequence of computational steps required for Phase I of the (n + 1)th time cycle calculations. To compute a given step for cell $\binom{j}{i}$ the results of the

previous step are required for certain cells close to $\binom{j}{i}$. One way to ensure this is to require that each of the computational steps is made for every cell in the mesh before the subsequent step is made for any one cell. As this is the simplest method to describe, it will be presented here even though it is clearly wasteful of computer storage space.

Step 1.1 The velocity components at the end of the n - th time cycle are evaluated at the cell boundaries. Ordinarily one uses the formulas

$$u^j_{i-1/2} = \frac{u^j_{i-1} + u^j_i}{2} \qquad v^j_{i-1/2} = \frac{v^j_{i-1} + v^j_i}{2} \tag{49}$$

$$u^{j-1/2}_i = \frac{u^{j-1}_i + u^j_i}{2} \qquad v^{j-1/2}_i = \frac{v^{j-1}_i + v^j_i}{2} . \tag{50}$$

If cell $\binom{j}{i}$ is empty at this instant, $M^j_i = 0$, no calculations are made for this cell during this step and no entries are made.

If cell $\binom{j}{i}$ has empty neighbors to the left or above then equations (49) and (50) are replaced:

If $M^j_{i-1} = 0$ then set

$$u^j_{i-1/2} = u^j_i \qquad v^j_{i-1/2} = v^j_i .$$

If $M^{j-1}_i = 0$ then set

$$u^{j-1/2}_i = u^j_i \qquad v^{j-1/2}_i = v^j_i .$$

Empty neighbors below or to the right cause no difficulty in this step.

If the cell is adjacent to the axis of symmetry, i = 1 and j = 0, 1, ..., $\gamma + 1$, then replace equation (49) by

$$u^j_{1/2} = 0 \qquad\qquad v^j_{1/2} = \frac{1}{8}(9v^j_1 - v^j_2).$$

The first relation follows from symmetry and the second from quadratic extrapolation with $(\partial v/\partial r)_{r=0} = 0$.

If the cell is adjacent to the top boundary, j = 1 and i = 0, 1, ..., $\beta + 1$, then replace equation (50) by

$$u_i^{1/2} = u_i^1 \qquad\qquad v_i^{1/2} = v_i^1.$$

No special provision need be made for cells adjacent to the right and bottom boundaries.

Step 1.2 The divergence of the velocity at the cell center is computed. Ordinarily one uses equation (30).

If cell $\binom{j}{i}$ is empty at this instant, $M_i^j = 0$, no calculations or entries are made.

If cell $\binom{j}{i}$ has empty neighbors to the right or below then in using (30) one must use special provisions:

If $M^j_{i+1} = 0$ then set

$$u^j_{i\,+\,1/2} = u^j_i.$$

If $M_i^{j+1} = 0$ then set

$$v^{j\,+\,1/2}_i = v^j_i.$$

No special provisions are required for cells adjacent to the axis of symmetry and the top boundary.

If the cell is adjacent to the right boundary, $i = \beta$ and $j = 0, 1, \ldots, \gamma + 1$, then use (30), but set

$$u^j_{\beta + 1/2} = u^j_{\beta}.$$

If the cell is adjacent to the bottom boundary, $j = \gamma$ and $i = 0, 1, \ldots, \beta + 1$, then use (30) but set

$$v_i^{\gamma + 1/2} = v_i^{\gamma}.$$

Step 1.3 The value at the cell center of the distortional strain-rate invariant D^2 is computed. Ordinarily one uses equation (31).

If cell $\binom{j}{i}$ is empty at this instant, $M_i^j = 0$, no entry is made.

If the cell has empty neighbors to the right or below, then in using (31) one makes the following provisions:

If $M_{i+1}^j = 0$, set

$$u^j_{i + 1/2} = u^j_i \qquad\qquad v^j_{i + 1/2} = v^j_i.$$

If $M_i^{j+1} = 0$, set

$$u_i^{j + 1/2} = u_i^j \qquad\qquad v_i^{j + 1/2} = v_i^j.$$

No special provisions are required if the cell is adjacent to the axis of symmetry or the top boundary.

If the cell is adjacent to the right boundary, $i = \beta$ and $j = 0, 1, \ldots, \gamma + 1$, then use (31) only set

$$u^j_{\beta + 1/2} = u^j_{\beta} \qquad\qquad v^j_{\beta + 1/2} = v^j_{\beta}.$$

If the cell is adjacent to the bottom boundary, $j = \gamma$ and $i = 0, 1, \ldots, \beta + 1$, then use (31) only set

$$u_i^{\gamma + 1/2} = u_i^{\gamma} \qquad v_i^{\gamma + 1/2} = v_i^{\gamma}.$$

Step 1.4 The value at the cell center of the strain-rate dependent viscosity coefficient is computed using (32). The functions $\eta(I, p)$ and $S(I, p)$ are written into the computer code as subroutines.

If cell $\binom{j}{i}$ is empty at this instant, $M_i^j = 0$, no calculation or entry is made. Otherwise, no special provisions are necessary.

Step 1.5 The cell center values of the quantities P, Q and r^2 are computed using equations (33), (34) and (35).

If cell $\binom{j}{i}$ is empty, $M_i^j = 0$, no entries are made.

If the cell has empty neighbors to the right or below, then in computing Q from (34) the following provisions are necessary:

If $M_{i+1}^j = 0$, set

$$v_{i + 1/2}^j = v_i^j.$$

If $M_i^{j+1} = 0$, set

$$u_i^{j + 1/2} = u_i^j.$$

No special provisions are required if the cell is adjacent to the axis of symmetry or the top boundary.

If the cell is adjacent to the right boundary, $i = \beta$ and $j = 0, 1, \ldots, \gamma + 1$, then the calculation of P and r^2 cause no difficulty but in using (34) to compute Q set

$$v_{\beta + 1/2}^j = v_{\beta}^j.$$

Similarly, if the cell is adjacent to the bottom boundary, $j = \gamma$ and $i = 0, 1, \ldots, \beta + 1$, then in using (34) to compute Q set

$$u_i^{\gamma + 1/2} = u_i^{\gamma}.$$

Step 1.6 The values of u/r, P and μ at the left cell boundary and the value of Q at the top cell boundary are computed. Ordinarily one uses the formulas

$$\left(\frac{u}{r}\right)^j_{i-1/2} = \frac{1}{2}\left[\frac{u^j_{i-1}}{(i - 3/2)h} + \frac{u^j_i}{(i - 1/2)h}\right] \tag{51}$$

$$P^j_{i-1/2} = \frac{P^j_{i-1} + P^j_i}{2} \tag{52}$$

$$\mu^j_{i-1/2} = \frac{\mu^j_{i-1} + \mu^j_i}{2} \tag{53}$$

$$Q^{j-1/2}_i = \frac{Q^{j-1}_i + Q^j_i}{2} . \tag{54}$$

If cell $\binom{j}{i}$ is empty at this instant, $M^j_i = 0$, no entries are made.

If cell $\binom{j}{i}$ has empty neighbors to the left or above then equations (51) through (54) are adjusted:

If $M^j_{i-1} = 0$ then set

$u^j_{i-1} = u^j_i$ in (51) to compute $\left(\frac{u}{r}\right)^j_{i-1/2}$

$P^j_{i-1/2} = 0$

$\mu^j_{i-1/2} = \mu^j_i$.

If $M_i^{j-1} = 0$ then set

$$Q_i^{j-1/2} = 0.$$

If the cell is adjacent to the axis of symmetry, i = 1 and j = 0, 1, ..., $\gamma + 1$, then replace equations (51), (52) and (53) by

$$\left(\frac{u}{r}\right)^j_{1/2} = 0$$

$$P^j_{1/2} = \frac{1}{8}(9\,P^j_1 - P^j_2)$$

$$\mu^j_{1/2} = \frac{1}{8}(9\,\mu^j_1 - \mu^j_2).$$

If the cell is adjacent to the top boundary, j = 1 and i = 0, 1, ..., $\beta + 1$, then replace (54) with

$$Q_i^{1/2} = Q_i^1.$$

No special provisions are required if the cell is adjacent to the right and bottom boundaries.

Step 1.7 The cell center value of the tentative new radial velocity, $\tilde{u}_i^j$, is computed using equation (28).

If cell $\binom{j}{i}$ is empty at this state, $M_i^j = 0$, no calculation or entry is made.

If cell $\binom{j}{i}$ has empty neighbors to the left, to the right or below then special provisions are required in using (28):

If $M_{i-1}^j = 0$ then set

$$u_{i-1}^j = u_i^j.$$

If $M^j_{i+1} = 0$ then set

$$P^j_{i+1/2} = 0$$

$$\mu^j_{i+1/2} = \mu^j_i$$

$$u^j_{i+1} = u^j_i$$

$$\left(\frac{u}{r}\right)^j_{i+1/2} = \frac{u^j_i}{2h}\left[\frac{1}{i-1/2} + \frac{1}{i+1/2}\right] .$$

If $M^{j+1}_i = 0$ then set

$$Q^{j+1/2}_i = 0.$$

An empty neighbor above the cell $\binom{j}{i}$ causes no difficulty.

If the cell is adjacent to the axis of symmetry, $i = 1$ and $j = 0, 1, \ldots, \gamma + 1$, then in using (28) set

$$u^j_0 = -u^j_1.$$

If the cell is adjacent to the right boundary, $i = \beta$ and $j = 0, 1, \ldots, \gamma + 1$, then in using (28) set

$$P^j_{\beta+1/2} = P^j_\beta$$

$$\mu^j_{\beta+1/2} = \mu^j_\beta$$

$$u^j_{\beta+1} = u^j_\beta$$

$$\left(\frac{u}{r}\right)^j_{\beta+1/2} = \frac{u^j_\beta}{2h}\left[\frac{1}{\beta-1/2} + \frac{1}{\beta+1/2}\right] .$$

If the cell is adjacent to the bottom boundary, $j = \gamma$ and $i = 0, 1, \ldots, \beta + 1$, then in using (28) set,

$$Q_i^{\gamma + 1/2} = Q_i^{\gamma}.$$

Step 1.8 Compute the value of (rQ) at the left cell boundary and the values of $\overline{P}$ and μ at the top cell boundaries. Ordinarily we use the equations

$$(rQ)^j_{i-1/2} = \frac{h}{2}\left[(i - 3/2)\, Q^j_{i-1} + (i - 1/2)\, Q^j_i\right] \tag{55}$$

$$P_i^{j-1/2} = \frac{P_i^{j-1} + P_i^j}{2} \tag{56}$$

$$\mu_i^{j-1/2} = \frac{\mu_i^{j-1} + \mu_i^j}{2} \quad . \tag{57}$$

If cell $\begin{pmatrix} j \\ i \end{pmatrix}$ is empty, $M_i^j = 0$, no calculations or entries are made.

If cell $\begin{pmatrix} j \\ i \end{pmatrix}$ has empty neighbors to the left or above then the following provisions are made:

If $M^j_{i-1} = 0$ then set

$$(rQ)^j_{i-1/2} = 0.$$

If $M_i^{j-1} = 0$ then set

$$P_i^{j-1/2} = 0$$

$$\mu_i^{j-1/2} = \mu_i^j.$$

Empty neighbors to the right or below cause no trouble during this step.

If the cell is adjacent to the axis of symmetry, i = 1 and j = 0, 1, ..., γ + 1, then replace equation (55) by

$$(r\Omega)^{j}_{1/2} = 0.$$

Adjacent to the top boundary, j = 1 and i = 0, 1, ..., β + 1, replace equations (56) and (57) with

$$P_i^{1/2} = P_i^1$$

$$\mu_i^{1/2} = \mu_i^1.$$

No special provisions are required for cells adjacent to the right and bottom boundaries.

Step 1.9 The cell center values of the tentative new axial velocity, $\tilde{v}_i^j$, is computed using equation (29).

If cell $\binom{j}{i}$ is empty, $M_i^j = 0$, no calculation or entry is made.

If cell $\binom{j}{i}$ has empty neighbors to the right, above, or below, then special provisions are required in using (29):

If $M_{i+1}^j = 0$ then set

$$(r\Omega)^{j}_{i+1/2} = 0.$$

If $M_i^{j-1} = 0$ then set

$$v_i^{j-1} = v_i^j.$$

If the cell is adjacent to the bottom boundary, $j = \gamma$ and $i = 0, 1, \ldots, \beta + 1$, then in using (28) set,

$$Q_i^{\gamma + 1/2} = Q_i^{\gamma}.$$

Step 1.8 Compute the value of (rQ) at the left cell boundary and the values of $\overline{P}$ and μ at the top cell boundaries. Ordinarily we use the equations

$$(rQ)^j_{i-1/2} = \frac{h}{2}\left[(i - 3/2)\, Q^j_{i-1} + (i - 1/2)\, Q^j_i\right] \tag{55}$$

$$P_i^{j-1/2} = \frac{P_i^{j-1} + P_i^j}{2} \tag{56}$$

$$\mu_i^{j-1/2} = \frac{\mu_i^{j-1} + \mu_i^j}{2} \quad . \tag{57}$$

If cell $\begin{pmatrix} j \\ i \end{pmatrix}$ is empty, $M_i^j = 0$, no calculations or entries are made.

If cell $\begin{pmatrix} j \\ i \end{pmatrix}$ has empty neighbors to the left or above then the following provisions are made:

If $M^j_{i-1} = 0$ then set

$$(rQ)^j_{i-1/2} = 0.$$

If $M_i^{j-1} = 0$ then set

$$P_i^{j-1/2} = 0$$

$$\mu_i^{j-1/2} = \mu_i^j.$$

Empty neighbors to the right or below cause no trouble during this step.

If $M_i^{j+1} = 0$ then set

$$P_i^{j+1/2} = 0$$

$$\mu_i^{j+1/2} = \mu_i^j$$

$$v_i^{j+1} = v_i^j \quad .$$

An empty neighbor to the left of cell $\binom{j}{i}$ causes no difficulty.

If the cell is adjacent to the top boundary, $j = 1$ and $i = 0, 1, \ldots, \beta + 1$, then in using (29) set

$$v_i^0 = v_i^1 \quad .$$

If the cell is adjacent to the right boundary, $i = \beta$ and $j = 0, 1, \ldots, \gamma + 1$, then in using (29) set

$$(r\Omega)_{\beta + 1/2}^j = h\beta \ \Omega_\beta^j .$$

If the cell is adjacent to the bottom boundary, $j = \gamma$ and $i = 0, 1, \ldots, \beta + 1$, then in using (29) set

$$P_i^{\gamma+1/2} = P_i^\gamma$$

$$\mu_i^{\gamma+1/2} = \mu_i^\gamma$$

$$v_i^{\gamma+1} = v_i^\gamma .$$

No special provision is required for the cells adjacent to the axis of symmetry.

Step 1.10 Compute the cell center values of the mean velocity components according to the relations

$$\hat{u}_i^j = \frac{1}{2}\left(u_i^j + \tilde{u}_i^j\right) \qquad \hat{v}_i^j = \frac{1}{2}\left(v_i^j + \tilde{v}_i^j\right). \tag{58}$$

If cell $\binom{j}{i}$ is empty at this stage, $M_i^j = 0$, no calculations or entries are made. Otherwise there are no special provisions required.

Step 1.11 The mean velocity components are evaluated at the cell boundaries. Ordinarily one uses the formulas

$$\hat{u}_{i-1/2}^j = \frac{\hat{u}_{i-1}^j + \hat{u}_i^j}{2} \qquad \hat{v}_{i-1/2}^j = \frac{\hat{v}_{i-1}^j + \hat{v}_i^j}{2} \tag{59}$$

$$\hat{u}_i^{j-1/2} = \frac{\hat{u}_i^{j-1} + \hat{u}_i^j}{2} \qquad \hat{v}_i^{j-1/2} = \frac{\hat{v}_i^{j-1} + \hat{v}_i^j}{2} \; . \tag{60}$$

If cell $\binom{j}{i}$ is empty, $M_i^j = 0$, no calculations or entries are made. Otherwise, the same special provisions that are detailed in Step 1.1 are required here; only with u and v replaced by $\hat{u}$ and $\hat{v}$.

Step 1.12 The divergence of the mean velocity at the cell center is computed. Ordinarily one uses the formula (46).

If cell $\binom{j}{i}$ is empty, $M_i^j = 0$, no calculation or entry is made. Otherwise, the same special provisions that are detailed in Step 1.2 are required here; only with u and v replaced by $\hat{u}$ and $\hat{v}$.

Step 1.13 The cell center values of Ψ and $\hat{D}^2$ are computed using formulas (39) and (47).

If cell $\binom{j}{i}$ is empty, $M_i^j = 0$, no calculations or entries are made. No other special provisions are necessary for Ψ. The same special provisions that are detailed in Step 1.3 for the computation of D^2 are required here in computing $\hat{D}^2$ except that u and v are replaced by $\hat{u}$ and $\hat{v}$.

Step 1.14 The cell center value of $\hat{\mu}$ is computed, ordinarily one uses formula (48).

If cell $\begin{pmatrix} j \\ i \end{pmatrix}$ is empty at this stage, $M_i^j = 0$, no entry is made. Otherwise, no special provisions are required.

Step 1.15 The cell center values of V_{rr}, V_{rz} and V_{zz} are computed, ordinarily using equations (42), (45) and (44) respectively.

If cell $\begin{pmatrix} j \\ i \end{pmatrix}$ is empty, $M_i^j = 0$, no calculations or entries are made.

If the cell has empty neighbors to the right or below then the following provisions are required:

If $M_{i+1}^j = 0$, set

$\hat{u}_{i+1/2}^j = \hat{u}_i^j$ when using (42)

$\hat{v}_{i+1/2}^j = \hat{v}_i^j$ when using (45).

If $M_i^{j+1} = 0$, set

$\hat{u}_i^{j+1/2} = \hat{u}_i^j$ when using (45)

$\hat{v}_i^{j+1/2} = \hat{v}_i^j$ when using (44).

No special provisions are required if the cell is adjacent to the axis of symmetry or the top boundary.

If the cell is adjacent to the right boundary, $i = \beta$ and $j = 0, 1, \ldots, y + 1$, then set

$\hat{u}_{\beta+1/2}^j = \hat{u}_\beta^j$ when using (42)

$\hat{v}_{\beta+1/2}^j = \hat{v}_\beta^j$ when using (45).

If the cell is adjacent to the bottom boundary, $j = \gamma$ and $i = 0, 1, \ldots, \beta + 1$, then set

$$\hat{u}_i^{\gamma+1/2} = \hat{u}_i^{\gamma} \qquad \text{when using (45)}$$

$$\hat{v}_i^{\gamma+1/2} = \hat{v}_i^{\gamma} \qquad \text{when using (44).}$$

Step 1.16 Compute the cell center value of $V_{\theta\theta}$ and the left cell boundary value of Λ. Ordinarily one uses formulas (43) and (40) respectively.

If the cell is empty, $M_i^j = 0$, no calculations or entries are made.

If cell $\binom{j}{i}$ has an empty neighbor to the left, i.e., $M_{i-1}^j = 0$, then replace (40) by

$$\Lambda_{i-1/2}^j = 0.$$

If the cell is adjacent to the axis of symmetry, $i = 1$ and $j = 0, 1, \ldots, \gamma + 1$, then replace (40) by

$$\Lambda_{1/2}^j = 0.$$

Here we have taken the average of the first two terms and the average of the last two terms of (40) to vanish independently, since the radial velocity and the shear stress both vanish at the axis of symmetry.

No other special provisions are required for $\Lambda_{i-1/2}^j$ and none at all are required for $(V_{\theta\theta})_i^j$.

Step 1.17 Compute the cell center values of V_{max} and Γ, and the upper cell boundary value of Ω. Ordinarily one uses formula (38) for Γ, formula (41) for Ω and the following formula for V_{max}:

$$\left(V_{max}\right)_i^j = \max \left\{ \left| \left(V_{rr}\right)_i^j \right| , \left| \left(V_{\theta\theta}\right)_i^j \right| , \left| \left(V_{zz}\right)_i^j \right| \right\} . \qquad (61)$$

If the cell is empty, $M_i^j = 0$, no calculations or entries are made.

If cell $\binom{j}{i}$ has an empty neighbor above, i.e., $M_i^{j-1} = 0$, then replace (41) by

$$\Omega_i^{j-1/2} = 0.$$

If cell $\binom{j}{i}$ is adjacent to the top boundary, $j = 1$ and $i = 0, 1, \ldots, \beta + 1$, then replace (41) by

$$\Omega_i^{1/2} = \hat{u}_i^1 (V_{rz})_i^1 + \hat{v}_i^1 (V_{zz})_i^1.$$

No other special provisions are required for $\Omega_i^{j-1/2}$ and none at all are required for Γ_i^j and V_{max}.

Step 1.18 Compute the upper cell boundary values of V_{rz} and V_{zz}. Ordinarily one uses the formulas

$$(V_{rz})_i^{j-1/2} = \frac{(V_{rz})_i^{j-1} + (V_{rz})_i^j}{2} \tag{62}$$

$$(V_{zz})_i^{j-1/2} = \frac{(V_{zz})_i^{j-1} + (V_{zz})_i^j}{2} . \tag{63}$$

If cell $\binom{j}{i}$ is empty at this stage, $M_i^j = 0$, no calculations or entries are made.

If cell $\binom{j}{i}$ has an empty neighbor above, i.e., $M_i^{j-1} = 0$, then set

$$(V_{rz})_i^{j-1/2} = 0$$

$$(V_{zz})_i^{j-1/2} = 0.$$

If the cell is adjacent to the top boundary, $j = 1$ and $i = 0, 1, \ldots, \beta + 1$, then replace (62) and (63) by

$$(V_{rz})^{1/2}_i = (V_{rz})^1_i$$

$$(V_{zz})^{1/2}_i = (V_{zz})^1_i \quad .$$

No other special provisions are required.

Step 1.19 Compute the left cell boundary values of V_{rr} and V_{rz}. Ordinarily one uses the formulas

$$(V_{rr})^j_{i-1/2} = \frac{(V_{rr})^j_{i-1} + (V_{rr})^j_i}{2} \tag{64}$$

$$(V_{rz})^j_{i-1/2} = \frac{(V_{rz})^j_{i-1} + (V_{rz})^j_i}{2} \quad . \tag{65}$$

If the cell is empty at this stage, $M^j_i = 0$, no calculations or entries are made.

If the cell has an empty neighbor to the left, i.e., $M^j_{i-1} = 0$, then set

$$(V_{rr})^j_{i-1/2} = 0$$

$$(V_{rz})^j_{i-1/2} = 0.$$

If the cell is adjacent to the axis of symmetry, i = 1 and j = 0, 1, ..., $y + 1$, then replace (64) and (65) by

$$(V_{rr})^{j}_{1/2} = \frac{1}{8}(9\ V_1^j - V_2^j)$$

$$(V_{rz})^{j}_{1/2} = 0.$$

No other special provisions are required.

Step 1.20 The tentative new specific internal energy is computed using equation (37).

If the cell is empty, $M_i^j = 0$, no calculations or entries are made.

If cell $\binom{j}{i}$ has empty neighbors to the right or below then in using (37) one must make special provisions:

If $M^j_{i+1} = 0$ then set

$$\Lambda^{j}_{i+1/2} = 0$$

$$(V_{rr})^{j}_{i+1/2} = 0$$

$$(V_{rz})^{j}_{i+1/2} = 0.$$

If $M_i^{j+1} = 0$ then set

$$\Omega^{j+1/2}_{i} = 0$$

$$(V_{rz})^{j+1/2}_{i} = 0$$

$$(V_{zz})^{j+1/2}_{i} = 0.$$

If the cell is adjacent to the right boundary, $i = \beta$ and $j = 0, 1, \ldots, \gamma + 1$, then use (37) to compute $\tilde{I}$ but set

$$\Lambda^{j}_{\beta+1/2} = \Lambda^{j}_{\beta}$$

$$(V_{rr})^{j}_{\beta+1/2} = (V_{rr})^{j}_{\beta}$$

$$(V_{rz})^{j}_{\beta+1/2} = (V_{rz})^{j}_{\beta}.$$

If the cell is adjacent to the bottom boundary, $j = \gamma$ and $i = 0, 1, \ldots, \beta + 1$, then in using (37) set

$$\Omega^{\gamma+1/2}_{i} = \Omega^{\gamma}_{i}$$

$$(V_{rz})^{\gamma+1/2}_{i} = (V_{rz})^{\gamma}_{i}$$

$$(V_{zz})^{\gamma+1/2}_{i} = (V_{zz})^{\gamma}_{i}.$$

Note, if a negative value for the tentative specific internal energy is computed per cell $\binom{j}{i}$ by the above procedure, set $\tilde{I}^{j}_{i} = 0$.

Step 1.21 The tentative new cellwise velocity components are recomputed using the formulas

$$\tilde{u}^{j}_{i} = 2\hat{u}^{j}_{i} - u^{j}_{i}$$

$$\tilde{v}^{j}_{i} = 2\hat{v}^{j}_{i} - v^{j}_{i}.$$

If cell $\binom{j}{i}$ is empty, $M^{j}_{i} = 0$, no calculations or entries are made.

No other special provisions are required.

PHASE II - CALCULATIONS

At the end of Phase I there are stored in machine-memory fourteen quantities for every non-empty cell $\begin{pmatrix} j \\ i \end{pmatrix}$. Table V shows these, together with the quantities which replace them during the sequence of the Phase II calculations. The mass particles will now be moved and this effect will be taken into account in recomputing the velocity and specific internal energy as detailed below.

Step 2. 1 This is a preparatory step in which the tentative energy and momentum are totaled over all the particles in the cell at the end of Phase I:

$$\tilde{E}_i^j = M_i^j \left\{ \tilde{I}_i^j + \frac{1}{2} \left[(\tilde{u}_i^j)^2 + (\tilde{v}_i^j)^2 \right] \right\} \tag{66}$$

$$\tilde{R}_i^j = M_i^j \, \tilde{u}_i^j \tag{67}$$

$$\tilde{Z}_i^j = M_i^j \, \tilde{v}_i^j. \tag{68}$$

If cell $\begin{pmatrix} j \\ i \end{pmatrix}$ is empty, $M_i^j = 0$, no calculations are performed and no entries are made.

Step 2. 2 The quantities in the four indicated registers, nos. 10, 11, 12 and 13, of each cell are replaced by zero. This preparatory step is carried out even for the empty cells.

Step 2. 3 The particles are moved; new values for the total cellwise mass, energy, and components of momentum are computed. To perform this step one goes through the particles (that remain in the system at this stage) one-by-one, computing the new location of each and the contributions of each to the new values of the cellwise quantities. The contributions are permitted to accumulate to the final total values of M', E', R' and Z'.

Thus, suppose the particles have been labeled and that the ν - th particle is of mass m_ν and its coordinates at the end n - th time cycle are (r_ν, z_ν). The substeps associated with the motion of the ν - th particle during Step 2. 3 are shown more explicitly in the schematic of Table VI. They are also described below. After the calculations associated with the ν - th particle have

been completed the floating storage capacity is available for the calculations associated with the $(\nu + 1)$th particle, etc.

(Substep ν . 1) The indices of the cell in which the ν - th particle is located at the end of the n - th time cycle are computed by the formulas

$$\begin{aligned} &[\text{largest integer} \leq r_\nu/h] \\ &[\text{largest integer} \leq z_\nu/k] \end{aligned} \tag{69}$$

These integral values are then stored in the Floating Storage.

(Substep ν . 2) The velocity components of the ν - th particle are computed by the "area averaging" formulas presented in Appendix B. Their values, u_ν and v_ν, are then stored in Floating Storage.

(Substep ν . 3) The new position coordinates are computed by the formulas

$$\begin{aligned} r'_\nu &= r_\nu + u_\nu \delta t \\ z'_\nu &= z_\nu + v_\nu \delta t. \end{aligned} \tag{70}$$

The values r_ν' and z_ν' then replace the values r_ν and z_ν in the ν - th Particle Storage.

(Substep ν . 4) The indices of the cell in which the ν - th particle is located at the end of the $(n + 1)$th time cycle are computed by the formulas

$$\begin{aligned} &[\text{largest integer} \leq r'_\nu/h] \\ &[\text{largest integer} \leq z'_\nu/k]. \end{aligned} \tag{71}$$

These integers then replace r_ν' and z_ν' in the Floating Storage.

(Substep ν . 5) The contribution which the ν - th particle makes to the total mass, energy, and momentum in the $\binom{j^*}{i^*}$ cell are now computed using the formulas

$$\Delta M_{i^*}^{j^{*'}} = m_\nu \tag{72}$$

$$\Delta E_{i^*}^{j^{*'}} = \frac{m_\nu}{M_i^j} \tilde{E}_i^j \tag{73}$$

$$\Delta R_{i^*}^{j^{*'}} = \frac{m_\nu}{M_i^j} \tilde{R}_i^j = m_\nu \, \tilde{u}_i^j \tag{74}$$

$$\Delta Z_{i^*}^{j^{*'}} = \frac{m_\nu}{M_i^j} \tilde{Z}_i^j = m_\nu \, \tilde{v}_i^j \quad . \tag{75}$$

If both $0 < i^* < \beta + 1$ and $0 < j^* < \gamma + 1$ the particle still remains within the mesh and these contributions are then added to the quantities already present in the corresponding memory registers (10, 11, 12 and 13 respectively) of cell $\binom{j^*}{i^*}$. If either i* or j* violates its above inequality, the particle will have left the mesh and no entry is made in any cellwise storage.

Step 2. 4 The cellwise density and the velocity components at the end of the (n + 1)th time cycle are computed:

$$\rho_i^{j'} = \frac{M_i^{j'}}{2\pi (i - 1/2) h^2 k} \tag{76}$$

$$u_i^{j'} = R_i^{j'} \Big/ M_i^{j'} \tag{77}$$

$$v_i^{j'} = Z_i^{j'} \Big/ M_i^{j'} \, . \tag{78}$$

Also insert the value of $M_i^{j'}$ into the first register.

If cell $\begin{pmatrix} j \\ i \end{pmatrix}$ is empty, i.e., $M_i^{j'} = 0$, at this stage no calculations or entries are made. No other provisions are required.

Step 2.5 The cellwise specific internal energy at the end of (n + 1)th time cycle is computed:

$$I_i^{j'} = \frac{E_i^{j'}}{M_i^{j'}} - \frac{1}{2}\left[(u_i^{j'})^2 + (v_i^{j'})^2\right]. \tag{79}$$

If the cell is empty, $M_i^{j'} = 0$, no computation or entry is made. If (79) gives a negative value set $I_i^{j'} = 0$.

Step 2.6 The cellwise value for the tentative new pressure is computed under the temporary assumption that no material fracture occurs in cell $\begin{pmatrix} j \\ i \end{pmatrix}$ during the (n + 1)th time cycle. According to (19) we have the following:

$$\begin{aligned} \tilde{p}_i^j &= f(\rho_i^{j'}, I_i^{j'}) \qquad \text{if } \zeta_i^{j'} = \frac{\rho_i^{j'}}{\rho_o} - 1 \geq 0 \\ &= h(\rho_i^{j'}, I_i^{j'}) \qquad \text{if } \zeta_i^{j'} = \frac{\rho_i^{j'}}{\rho_o} - 1 < 0 \end{aligned} \tag{80}$$

If cell $\begin{pmatrix} j \\ i \end{pmatrix}$ is empty, $M_i^{j'} = 0$, no entry is made; otherwise no special provisions are required. The functions $f(\rho, I)$ and $h(\rho, I)$ are written into the computer code as subroutines.

Step 2.7 The cellwise pressure at the end of the (n + 1)th time cycle is computed. According to hypotheses (20) and (24) we have the following:

$$\begin{aligned} p_i^{j'} &= 0 \text{ if } \tilde{p}_i^j < 0 \\ &\quad \text{and } (V_{max})_i^j \geq \frac{1}{\omega}\left\{\lambda - \left[\frac{1}{c} I_i^{j'} - 300\right] \ln \delta t/t_o\right\} \\ &= \tilde{p}_i^j \text{ otherwise} \end{aligned} \tag{81}$$

If cell $\begin{pmatrix} j \\ i \end{pmatrix}$ is empty, $M_i^{j'} = 0$, no entry is made; otherwise no special provisions are required. The fracture criterion (81) is also incorporated into the computer code as a subroutine.

At the end of Step 2.7, the information in the machine memory is in such a form that the computations for the (n + 2)th time cycle may begin immediately. However, first making some subsidiary calculations is helpful.

PHASE III - CALCULATIONS

In the impact problem the total mass, total axial momentum and the total energy of the projectile-target system are rigorously conserved:

$$M_s = M'_s = \text{Mass of System} \tag{82}$$

$$Z_s = Z'_s = \frac{\pi}{4} H^2 L \rho_o v_o \tag{83}$$

$$E_s = E'_s = \frac{\pi}{8} H^2 L \rho_o v_o^2. \tag{84}$$

These quantities and the total radial momentum of the system, R_s, will be computed and monitored; such checks serve to indicate machine or coding errors.*

An interesting calculation is to obtain the above quantities for the projectile alone,

$$M_p = M'_p = \frac{\pi}{4} H^2 L \rho_o, \; Z_p, \; E_p, \; R_p, \tag{85}$$

and the location of the projectile-target interface:

$$\xi'_i = \left\{ \begin{array}{l} \text{Maximum value of the axial coordinates of all those} \\ \text{projectile particles that lie within the i-th column of} \\ \text{cells at the end of the (n + 1)th time cycle.} \end{array} \right\} \tag{86}$$

---

*A restart procedure will also be written into the program so that a machine error at any stage of the calculation will not require recomputing from the beginning of the problem.

This information is helpful in delineating the primary flow (during which the projectile is expended) from the secondary flow (during which the cratering mechanism is essentially a cavitation process.)

a) Total System Functionals

To compute the total mass of the projectile-target system, M_s, it is only necessary to cumulate the masses of the particles within the mesh and the masses of those that have left the mesh by crossing one of the three continuative boundaries. Each of the departing particles will also carry its contributions to E_s, R_s, Z_s outside the mesh. In addition, however, energy and momentum are lost across the continuative boundaries by diffusion once the disturbance produced by the impact is propagated to the mesh boundary. Hence, to monitor E_s, R_s, and Z_s throughout the computation it is necessary to provide for loss across the boundaries both by particle motion and by diffusion:

$$M'_s = (M'_s)_{in} + (M'_s)_{out} \tag{87}$$

$$E'_s = (E'_s)_{in} + (E'_s)_{out} \quad \text{where } (E'_s)_{out} = (E'_s)^{diff.}_{out} + (E'_s)^{part.}_{out} \tag{88}$$

$$R'_s = (R'_s)_{in} + (R'_s)_{out} \quad \text{where } (R'_s)_{out} = (R'_s)^{diff.}_{out} + (R'_s)^{part.}_{out} \tag{89}$$

$$Z'_s = (Z'_s)_{in} + (Z'_s)_{out} \quad \text{where } (Z'_s)_{out} = (Z'_s)^{diff.}_{out} + (Z'_s)^{part.}_{out} \tag{90}$$

The schematic in Table VII depicts the processes by which the above quantities are cumulated from the contributions carried by the particles and by diffusion from cells just inside continuative boundaries. The contributions carried by the ν-th particle, whether it remains within or departs from the mesh during the (n + 1) th time cycle, are shown explicitly. The particle contributions are actually cumulated during Step 2.3. The losses by diffusion of E', R', Z', across the boundary of cell $\binom{j}{i}$, with $i = \beta$ or $j = 1$ or $j = \gamma$, are denoted by

$$\Delta^j_i (E'_s)^{diff.}_{out} \qquad \Delta^j_i (R'_s)^{diff.}_{out} \qquad \Delta^j_i (Z'_s)^{diff.}_{out} \tag{91}$$

The total diffusive losses are given by

$$( )_{out}^{diff.} = \sum_{\substack{\text{Cells at} \\ \text{Cont. Bdry.}}} \Delta_i^j ( )_{out}^{diff.}, \tag{92}$$

where the contributions (91) are computed by the formulas presented in Appendix C. The contributions to the diffusive losses of momentum and energy are actually cumulated during Steps 1.6 and 1.16, respectively, as indicated in Table VII.

These calculations are therefore not made subsequent to Phase II but are cumulated during both Phases I and II of the time cycle. At the start of each time cycle the register in which the contributions to $( )_{in}$ are to be cumulated will be zero, but each register in which the contributions to $( )_{out}$ are to be cumulated may be non-zero, since it includes the losses by particle motion and by diffusion during the previous n time cycles.

At the end of the (n + 1) th sweep through the cells and the particles, that part of each functional which remains within the mesh, $( )_{in}$, and that part which has left the mesh, $( )_{out}$, are entered individually. In the last substep shown in Table VII these corresponding subtotals are combined according to (87), ..., (90).

b) Delineation of Projectile

The functionals (85) and (86) are of interest only during the first stages of the cratering process. Therefore, no provision for diffusive losses will be made and these functionals will lose their significance in the later time cycles.

The corresponding cumulation process for the projectile material is depicted in the schematic of Table VIII. In this case one rejects all particles of the target material and then cumulates the contributions individually according to whether the particle remains within the mesh or is outside. Finally, the corresponding contributions are combined to give

$$M'_p = (M'_p)_{in} + (M'_p)_{out} \tag{93}$$

$$E'_p = (E'_p)_{in} + (E'_p)_{out} \tag{94}$$

$$R'_p = (R')_{p\,in} + (R')_{p\,out} \tag{95}$$

$$Z'_p = (Z')_{p\,in} + (Z')_{p\,out}. \tag{96}$$

Moreover, the projectile-target interface, defined by (86), is computed during this sweep in the manner depicted in Table VIII; η_i denotes the maximum new axial coordinate of all the first (ν - 1) particles that lie in the i - th column of cells.

c) Axial Shock Wave

Along the axis of symmetry the solution is identical to that of the impact between two semi-infinite bodies (under corresponding conditions) until rarefaction waves arrive from the edge of the projectile-target interface. The comparison of the location, amplitude, and velocity of the shock front with the one-dimensional solutions of Reference 6 gives a further check on the accuracy of the calculations during the early stages after impact.

CHANGE OF NET SIZE

As time goes on the size of the crater increases and the stress wave propagates further into the target. More target material must then be covered by the calculation mesh than is necessary at earlier times. As the dimensions of the disturbances increase, however, sufficient resolution may be obtained by using a larger net size, in both time and space, than was permissible during the initial stages of the process. It will therefore become advantageous to repartition the system during the course of a computational run.

a) Calculation of Time Step

The length of the time step δt may be varied; a smaller value is required during the early stages of the cratering mechanism than at a subsequent time when the particle velocity has decreased. In the present program it is computed for each step from the data of the previous time step. The idea is to specify an integer as the maximum number of particles that will move a distance so large that at the end of the time interval the particle is not in an adjacent (or identical) cell. The specified integer represents the maximum number of times that condition (B-1) of Appendix B may be violated.

b) Repartition of Space Mesh*

In rezoning the space mesh it is convenient to choose the original number of particles per cell, N, to be a perfect square. Since the optimum value of N is apparently between 3 and 9† it is natural to set

$$N = 4$$

in the present part of the formulation since an increase in the courseness of the mesh by a factor of nine may well be too abrupt. An additional advantage of the choice N = 4 is that for the same machine-memory capacity it permits smaller values of h and k which in turn decrease the effect of the artificial dissipative terms inherent to the method (Reference 33).

Assume that in the existing space mesh there are an even number of columns and rows and that originally there were four mass particles in each of the cells, i.e., β and γ are even and N = 4. Also assume that sufficient machine storage space has been allotted to accommodate $4\beta \times \gamma$ particles. Then an enlarged space mesh may be introduced in which the linear dimensions of the cells are doubled, i.e., four of the original cells are combined to form a single cell of the new mesh (see Figure 9). The area covered by the space mesh may thereby be increased fourfold without increasing the number of cells in the mesh. The time increment may also be increased in the new mesh:

$$h \rightarrow 2h \qquad k \rightarrow 2k. \tag{97}$$

In the 75% of the mesh area which has been newly introduced, each cell is assigned four mass particles randomly distributed within the cell. The mass of each of these particles is given by (27) with substitutions (97) inserted, i.e., the mass of each is eight times those of a particle initially (t = 0) in one of the original mesh cells with the same radial index i.

In the remaining 25%, which is being repartitioned, the masses in the enlarged cells are computed in the following manner. Each quadrant (sub-cell) of an enlarged cell is precisely one of the original cells. The mass particles in each sub-cell are coalesced to form a single particle provided the sub-cell is not empty; if the sub-cell is empty before repartitioning the

*The properties of the projectile alone can no longer be isolated after repartitioning as some of the coalesced masses will contain both projectile and target material. The calculations depicted in Table VIII are thereby meaningless after repartitioning.

†See the discussion following equation (108).

corresponding quadrant of the enlarged cell remains empty. The position of the coalesced mass particle is taken to be the mass center of the particles in the corresponding sub-cell prior to coalescence:

$$r_\alpha = \frac{1}{M_\alpha} \sum_{\text{sub-cell } \alpha} m_\nu \, r_\nu \tag{98}$$

$$z_\alpha = \frac{1}{M_\alpha} \sum_{\text{sub-cell } \alpha} m_\nu \, z_\nu \qquad \left(M_\alpha = \sum_{\text{sub-cell } \alpha} m_\nu \right). \tag{99}$$

The values of M_α are available from the last cycle of calculations made prior to repartitioning.

The velocity of the mass particles in the newly introduced 75% of the net area may be assigned; it is zero in the present problem. The velocity of each of the coalesced masses in the original 25% of the area may be chosen in such a way as to conserve energy and momentum. Conservation of axial and radial momentum requires that the corresponding velocity components of the enlarged cell be given by

$$v = \frac{1}{M} \sum_{\alpha = 1}^{4} M_\alpha \, v_\alpha \tag{100}$$

$$u = \frac{1}{M} \sum_{\alpha = 1}^{4} M_\alpha \, u_\alpha \qquad \left(M = \sum_{\alpha = 1}^{4} M_\alpha \right). \tag{101}$$

The u_α and v_α denote the sub-cell velocity components and are available from the last cycle of calculations made prior to repartitioning.

To conserve total energy the specific internal energy of the enlarged cell must be computed from the relation

$$I = -\frac{1}{2}(u^2 + v^2) + \frac{1}{M}\sum_{\alpha=1}^{4} M_\alpha \left[I_\alpha + \frac{1}{2}(u_\alpha^2 + v_\alpha^2)\right]$$

$$= -\frac{1}{2}(u^2 + v^2) + \frac{1}{M}\sum_{\alpha=1}^{4} E_\alpha, \tag{102}$$

where the E_α denote the total energy in each of the sub-cells composing the enlarged cell; these values are available from the last cycle of computations made prior to repartitioning. The density of material in the enlarged cell is computed from

$$\rho = \frac{M}{8\pi\, h\, k\, r}. \tag{103}$$

Here h x k are the dimensions of the original net and r denotes the radial distance to the center of the enlarged cell. The pressure in the enlarged cell is then computed according to the equation (according to relations 15 and 20):

$$\left.\begin{aligned} p &= f(\rho, I) \text{ if } \zeta \geq 0 \\ &= h(\rho, I) \text{ if } \zeta < 0 \\ &= 0 \text{ otherwise.} \end{aligned}\right\} \text{ and } \frac{1}{4}\sum_{\alpha=1}^{4} (V_{max})_\alpha < \sigma_{cr} \tag{104}$$

From (100) and (101) one may calculate the decrease in the total kinetic energy within the enlarged cell:

$$\Delta K.E. = \frac{1}{2} M (u^2 + v^2) - \frac{1}{2}\sum_{\alpha=1}^{4} M_\alpha (u_\alpha^2 + v_\alpha^2)$$

$$= \frac{-1}{2M}\sum_{\alpha,\alpha'=1}^{4} M_\alpha M_{\alpha'} \left[(u_\alpha - u_{\alpha'})^2 + (v_\alpha - v_{\alpha'})^2\right]$$

Hence,

$$\Delta K.E. \leq 0. \tag{105}$$

There is a loss in kinetic energy, ΔK. E. < 0, except for the case in which the velocities of the four sub-cells are identical. However, equation (102) insures that the total internal energy in the enlarged cell is increased by the same magnitude.

Actually the total radial momentum of the system is not conserved. This suggests an alternate procedure in which (91) and (92) are replaced by the conditions that the kinetic energy and internal energy are individually conserved:

$$u = \sqrt{- v^2 + \frac{1}{M} \sum_{\alpha = 1}^{4} M_\alpha \, (u_\alpha^2 + v_\alpha^2)} \tag{101'}$$

$$I = \frac{1}{M} \sum_{\alpha = 1}^{4} M_\alpha \, I_\alpha \, . \tag{102'}$$

In this case the total radial momentum in the enlarged cell is increased by

$$\Delta \text{R. M.} = Mu - \sum_{\alpha = 1}^{4} M_\alpha \, u_\alpha$$

$$= \left\{ \sum_{\alpha, \, \alpha' = 1}^{4} M_\alpha \, M_{\alpha'} \left[(u_\alpha - u_{\alpha'})^2 + (v_\alpha - v_{\alpha'})^2 \right] + \left(\sum_{\alpha = 1}^{4} M_\alpha \, u_\alpha \right)^2 \right\}^{1/2} - \sum_{\alpha = 1}^{4} M_\alpha \, u_\alpha \, .$$

Hence,

$$\Delta \text{R. M.} \geq 0. \tag{103'}$$

Equality holds only if the velocity of each of the four sub-cells is the same.

Which of these procedures gives the more accurate results will have to be decided by actual computational runs. In either case the computational method detailed in the preceding paragraphs may be carried out for subsequent time cycles using the enlarged mesh. It is only required that substitutions (97) be made in the equations governing each step of the calculations.

Mass, energy, or momentum that has previously departed from the mesh, either by particle motion or by diffusion across the mesh boundaries, cannot be recovered by the repartition process described above. Thus, the quantities that should be rigorously conserved during repartitioning are

$$(M_s)_{in},\ (E_s)_{in},\ (Z_s)_{in}$$

rather than

$$M_s,\ E_s,\ Z_s.$$

If the repartitioning is delayed too long the loss of M, E, R, Z across the continuative mesh boundaries will introduce large errors. To avoid this the computer program may be written to automatically repartition whenever the cumulative loss of any one of the four quantities exceeds a specified small fraction of the total quantity remaining inside the mesh.

COMPUTER PROGRAM (PICWICK)

The computational procedure described in the preceding sections taxes both the memory capacity and the speed of most computers. The particular programming logic selected depends upon the trade-off between computation time and storage, whichever is most advantageous for the particular computer used. The following is a brief description of the considerations that have led to PICWICK, a computer program for the IBM 7090 that uses only internal storage. No account has been taken of the possibility of using a high-speed magnetic disc for intermediate storage since none is presently available at either the General Electric Company or at the Eglin Air Force Base. The use of magnetic tape would be prohibitively slow.

STORAGE FOR CELLS

To compute a given step, in the Phase I and Phase II calculations, the results of the previous step for certain cells near to $\binom{j}{i}$ must be available. From a bookkeeping standpoint this is most simply accomplished by requiring that each computational step be made for every cell in the mesh before the subsequent step is made for any one cell. This straightforward procedure, depicted in Tables IV and V, would require a total of $14\beta\gamma$ storage locations for the cellwise quantities. This number would be required for the Phase I calculations and would also provide for the Phase II storage by "overlays". This simple procedure, however, is wasteful of machine storage space.

The required cellwise storage can be greatly reduced by carefully sequencing and by making use of movable storage. If computing time was of minor importance, the storage requirements could be reduced to $5\beta\gamma$ locations. A method has actually been worked out which accomplishes this by trading computing time for storage. This breaks down as follows: 5 locations per cell are needed in Phase I to store M, u, v, I and V_{max}, with r^2 "read out" in Phase I when called for. Modifications in the criterion for fracture could reduce this to 4 locations by eliminating the need to store V_{max}. In Phase II, 5 locations are needed to store M, u, v, I and p. The method would probably not be economical with the IBM 7090, but probably would be with the IBM 7030 ("Stretch").

To save time on the 7090 in the Phase II calculations an additional three locations per cell are required for ΔE, ΔR and ΔZ. Hence the total is eight per cell. Since the storage can be shared with Phase I the total cellwise storage required for the PICWICK program is $8\beta\gamma$.

STORAGE FOR PARTICLES

For each of the $N\beta\gamma$ particles one location is needed to store u, and one to store v. Since there are only $N\beta$ distinct masses all the masses can be stored in $N\beta$ locations by proper grouping. Therefore $2N\beta\gamma + N\beta \tilde{=} 2N\beta\gamma$ locations are apparently required for the particles. Unfortunately, however, books must be kept on the particles that have left the mesh. To do so requires $N\beta$ locations, which can be "shared" with the N locations required for the particle masses.

Therefore, $3N\beta\gamma$ locations are needed for the particle storage if particles leave the mesh and approximately $2N\beta\gamma$ are needed if they do not. The former is applicable to the present problem.

TOTAL PERMANENT STORAGE

The storage required for the program itself is quite large. For comparative purposes, however, the necessary total permanent storage is approximated by the sum of the cell and particle storage requirements for a β x γ cell mesh with originally N particles per cell. If the simple procedure of keeping books is followed the storage requirement would then be approximated by

$$S_1 = (14 + 3N)\beta\gamma \tag{106}$$

The more sophisticated bookkeeping procedures used in the PICWICK code reduce the total permanent storage required to

$$S_2 = (8 + 3N)\beta\gamma. \tag{107}$$

In order to obtain some estimate of the optimum number of particles per computational cell, in a memory limited computer such as the IBM 7090, the heuristic argument of Harlow (Reference 35) may be applied. Accordingly, one optimizes

$$Q_1 = \beta\gamma\sqrt{N} \quad \text{and} \quad Q_2 = (\beta\gamma)^{3/2}N \tag{108}$$

with S held constant. The first alternative gives equal weight to the Eulerian and Langrangian systems; the second choice gives a greater weight to the Eulerian system. Applied to S_1, the calculation yields 14/3 for the first alternative and 28/3 for the second. Applied to S_2 the results are 8/3 and 8 respectively.

The optimum number of particles per cell is apparently, therefore, from N = 3 to N = 9. For most of our calculations the choice of N = 4 is used as we have seen this to be especially convenient in repartitioning the space mesh – a desirable procedure if the cratering process is to be studied throughout its formation. If, indeed, four particles per cell are used, the IBM 7090 internal memory (32,000 registers) would be exhausted by a mesh of $\beta \times \gamma <$ 1230, about 30 by 40 cells, if the simple bookkeeping procedure leading to (106) is used. On the other hand, if the program storage requirement is approximated by (107) a mesh of $\beta \times \gamma < 1600$, about 35 by 45 cells would become feasible. The latter applies to the PICWICK program. This is very important because the nearly optimum resolution thus obtained is apparently just sufficient to make useful calculations possible without resorting to super computers such as Stretch.

CONCLUSIONS

A "debugged" computer program of the visco-plastic governing equations has been developed for axisymmetric hypervelocity impact between a projectile and target of the same material. The computational scheme requires the equation of state, the flow-resistance coefficient, and the fracture criteria for dynamic tri-axial stress conditions. Since none of these phenomenological relations have been firmly established by experiments under the severe conditions operative during hypervelocity impact, the proposed relations are considered tentative, and have been written into the program as sub-routines so th at they may be readily changed. The uncertainties involved are less important than the ability of the analysis to include and compare various proposed phenomenological relations.

In the special case that the flow resistance coefficient is set equal to zero and the effect of material strength is ignored, the governing equations reduce to the perfect fluid equations. In the first computer production runs, to be made with PICWICK at Eglin AFB, this case will be treated. This will provide a check with the calculations presented by Bjork (Reference 38).

A realistic theory must, however, include the effects of flow-resistance and fracture resistance. In the first runs in which these effects are included η and S will be assigned constant values. This will permit comparison of the results with those previously obtained for the case of normal impact between two semi-infinite iron bodies (Reference 6). During the early stages after impact the axisymmetric solution along the axis of symmetry should be in agreement with the one-dimensional solution obtained using the same values of η_o, S_o, and impact velocity. Subsequent runs will be made for copper and aluminum using the estimates (13) for η_o and handbook values for S_o.

The early production runs, in which the dependence of μ on the thermodynamic state is included, will investigate the effect of the temperature while neglecting the effect of the pressure. There are two reasons for this procedure. More experimental data are available concerning the effect of temperature on the flow-resistance of materials than the effect of pressure. Further, hypervelocity impact experiments in which the temperature of the target material was widely varied have shown that drastically different crater dimensions result; crater volumes of lead, cadmium, zinc, and copper were observed to increase by a factor of two to five when the target temperature was near the metal's melting point (Reference 39). Indeed, the inability of the perfect fluid model to account for these results was one of the factors that led us to develop the visco-plastic model of hypervelocity impact. In these computer runs the forms (8) and (14) will be used in which the parameters are approximated respectively from plastic wave propagation experiments and static yield tests carried out at elevated temperatures.

BIBLIOGRAPHY

1. Eichelberger, R.J., and Gehring, J.W., "Effects of Meteoroid Impacts on Space Vehicles", ARS Space Flight Report to the Nation, New York, October 9, 1961.

2. Riney, T.D., "A Visco-Plastic Model for Hypervelocity Impact", Quarterly Report No. 1, November 3, 1960 - February 2, 1961 (APGC-TN-61-16).

3. Riney, T.D., "Study of Equations Governing the Visco-Plastic Model", Quarterly Report No. 2, February 3, 1961-May 2, 1961 (APGC-TN-61-30).

4. Riney, T.D., "Numerical Investigation of One-Dimensional Visco-Plastic Model", Quarterly Report No. 3, May 3, 1961-September 2, 1961 (APGC-TN-61-43).

5. Riney, T.D., and Chernoff, P.R., "Inertial, Viscous, and Plastic Effects in High Speed Impact", Paper presented at the Fifth Symposium on Hypervelocity Impact in Denver, Colorado, October 31, 1961.

6. Riney, T.D., "Theory of High Speed Impact", Summary Report, November 3, 1960 - November 2, 1961 (APGC-TDR-62-20).

7. Riney, T.D., "Difference Scheme for Axisymmetric Impact Problem", Quarterly Progress Report No. 4, November 3, 1961 - February 2, 1962 (APGC-TDR-62-19).

8. Riney, T.D., "PIC Formulation of Visco-Plastic Model for Hypervelocity Impact", Quarterly Report No. 5, February 3, 1962 - May 2, 1962 (APGC-TDR-62-24).

9. Riney, T.D., "Constitutive Relations for Hypervelocity Impact", Quarterly Report No. 6, May 3, 1962 - August 2, 1962 (APGC-TDR-62-).

10. Gruntfest, I.J., "A Note on Thermal Feedback and the Fracture of Solids", Presented at International Conference on Fracture, Maple Valley, Washington, August 21-24, 1962.

11. Liquid Metals Handbook, Second Edition, June 1952, NAVEX, p. 733 (Rev.).

12. International Critical Tables, Vol. V, p. 7, 1929.

13. Shirdkovskiy, Y.G., "Certain Problems Related to the Viscosity of Fused Metals", NASA Technical Translation, F-88, March, 1962.

14. Jones, W.R.D., and Davies, J.B., "The Viscosity of Lead, Tin, and Their Alloys", Jour. Inst. Metals, Vol. 86, 1957-1958, pp. 164-166.

15. Dorn, J.E., "Some Fundamental Experiments on High Temperature Creep", Proceedings of a Symposium on Creep and Fracture of Metals at High Temperatures, National Physical Laboratory of Great Britain, May 31 - June 2, 1954, Published by H.M. Stationary Office, 1956.

16. Hauser, F.E., Simmons, J.A., and Dorn, J.E., "Strain-Rate Effects in Plastic Wave Propagation", Proceedings of Conference on Response of Metals to High Velocity Deformation, Estes Park, Colorado, July 11-12, 1960, Interscience Publishers, Inc., 1961.

17. Malvern, L.E., "The Propagation of Longitudinal Waves of Plastic Deformation in a Bar of Material Exhibiting a Strain-Rate Effect", Jour. Appl. Phys., Vol. 18, p. 203, 1951.

18. Perzyna, P., "Stress Waves in a Homogeneous Elastic-Visco-Plastic Medium", Arch. Mech. Stos., Vol. II, No. 4, 1959.

19. Alcoa Aluminum Handbook, Aluminum Company of America, Pittsburgh, Pa., 1957.

20. Bridgman, P.W., Studies in Large Plastic Flow and Fracture, Mc-Graw Hill Book Company, Inc., 1952.

21. Harlow, F.H., Personal Communication at Los Alamos Scientific Laboratory, July, 1962.

22. Zhurkov, S.N., and Sanfirova, T.P., "Relation Between Strength and Creep of Metals and Alloys", Journal of Technical Physics, USSR, Vol. 28, p. 1719, 1958.

23. Zhurkov, S.N., and Sanfirova, T.P., Doklady Akad, Nauk SSSR, Vol. 101, p. 237, 1955.

24. Zhurkov, S.N., "The Problem of Strength of Rigid Bodies" (In Russian), Vestnik Akad. Nauk SSSR, Vol. 11, p. 78, 1957.

25. Seitz, F., The Modern Theory of Solids, First Edition, McGraw-Hill Book Company, Inc., 1940, p. 111.

26. Perzyna, P., "The Constitutive Equations for Rate Sensitive Plastic Materials", Brown Univ. Div. Appl. Math., Tech. Rpt. No. 76, Contract NONR 562 (10), April, 1962.

27. Perzyna, P. "The Study of the Dynamic Behavior of Rate Sensitive Plastic Materials", Brown Univ. Div. Appl. Math, Tech Rpt. No. 77, Contract NONR 562 (10), May, 1962.

28. Hunter, S.C., "An Account of the Dynamic Properties of Solids (1961)", RARDE Memorandum (MX) 8/62, March, 1962.

29. Kolsky, H.G., "A Method for the Numerical Solution of Transient Hydrodynamic Shock Problems in Two Space Dimensions", Los Alamos Scientific Laboratory, LA-1867, April 1955.

30. Orlow, T., Piacesi, D. and Sternberg, H.M., "A Computer Program for the Analysis of Transient, Axially Symmetric, Explosion and Shock Dynamics Problems", Naval Ordnance Laboratory, NAVWEPS Report 7265, December, 1960.

31. Goad, W.B., "WAT: A Numerical Method for Two-Dimensional Unsteady Fluid Flow", Los Alamos Scientific Laboratory LAMS-2365, November, 1960.

32. Fromm, J.E., "Lagrangion Difference Approximation for Fluid Dynamics", Los Alamos Scientific Laboratory, LA-2535, June, 1961.

33. Evans, M.W., and Harlow, F.H., "The Particle-in-Cell Method for Hydrodynamic Calculations", Los Alamos Scientific Laboratory, LA-2139, November, 1957.

34. Harlow, F.H., "Two-Dimensional Hydrodynamic Calculations", Los Alamos Scientific Laboratory, LA-2301, September, 1959.

35. Harlow, F.H., "PIC Method for Fluid Dynamics Calculations" (To be published).

36. Harlow, F.H., and Meixner, B.D., "The Particle-and-Force Computing Method for Fluid Dynamics", Los Alamos Scientific Laboratory, LAMS-2567, October, 1961.

37. Serrin, James, "Mathematical Principles of Classical Fluid Mechanics", Encyclopedia of Physics Vol. VIII/1, Edited by S. Flugge, pp. 125-263, Springer-Verlag, 1959.

38. Bjork, R. L., "Effects of a Meteoroid Impact on Steel and Aluminum in Space", Technical Report P-1662, Rand Corporation, Eng. Division, Dec. 16, 1958.

39. Allison, F. E., Becker, K. R., and Vitali, R., "Effects of Target Temperature and Hypervelocity Cratering", Carnegie Institute of Technology, Quarterly Report No. 18, Contract No. DA-36-061-ORD-513, April 30, 1960.

APPENDIX A

Let ρ, p, $\bar{u} = (u, 0, v)$ and I denote the density, pressure, velocity, and specific internal energy respectively. Then the axisymmetric formulation of the visco-plastic equations may be written in the form (References 2 and 6):

$$\frac{\partial \rho}{\partial t} + u \frac{\partial \rho}{\partial r} + v \frac{\partial \rho}{\partial z} + \rho \operatorname{div} \bar{u} = 0 \tag{A-1}$$

$$\rho \left(\frac{\partial u}{\partial t} + u \frac{\partial u}{\partial r} + v \frac{\partial u}{\partial z} \right) = \frac{\partial}{\partial r} \left(P + 2 \mu (I, p, D) \frac{\partial u}{\partial r} \right) + 2 \mu (I, p, D) \frac{\partial}{\partial r} \left(\frac{u}{r} \right) + \frac{\partial Q}{\partial z} \tag{A-2}$$

$$\rho \left(\frac{\partial v}{\partial t} + u \frac{\partial v}{\partial r} + v \frac{\partial v}{\partial z} \right) = \frac{\partial}{\partial z} \left(P + 2 \mu (I, p, D) \frac{\partial v}{\partial z} \right) + \frac{1}{r} \frac{\partial}{\partial r} \left(rQ \right) \tag{A-3}$$

$$\rho \left(\frac{\partial I}{\partial t} + u \frac{\partial I}{\partial r} + v \frac{\partial I}{\partial z} \right) + p \operatorname{div} \bar{u} = \mu (I, p, D) D^2 \tag{A-4}$$

$$p = F (\rho, I) \tag{A-5}$$

where

$$\left.\begin{aligned} P &= - p - \frac{2}{3} \mu (I, p, D) \operatorname{div} \bar{u} \\ Q &= \mu (I, p, D) \left(\frac{\partial u}{\partial z} + \frac{\partial v}{\partial r} \right) \\ \mu &\equiv \mu (I, p, D) = \eta (I, p) + \frac{S(I, p)}{\sqrt{D^2 + \epsilon}} \\ \tau^2 &= D^2 \mu^2 \\ D^2 &= \left(\frac{\partial u}{\partial z} + \frac{\partial v}{\partial r} \right)^2 + 2 \left[\left(\frac{\partial u}{\partial r} \right)^2 + \left(\frac{u}{r} \right)^2 + \left(\frac{\partial v}{\partial z} \right)^2 \right] \\ &\quad - \frac{2}{3} (\operatorname{div} \bar{u})^2 \end{aligned}\right\} \tag{A-6}$$

$$\operatorname{div} \bar{u} = \frac{\partial u}{\partial r} + \frac{u}{r} + \frac{\partial v}{\partial z}$$

The introduction of the parameter $\epsilon > 0$ into the definition of the viscosity coefficient, $\mu(I, p, D)$ greatly simplifies the problem since it eliminates the moving surface of separation between the rigid and fluid regions of the medium. Thus r^2 is not necessarily $\geq r_0^2$. This not only simplifies the calculations, but is also more realistic because the shearing stresses now depend upon the strain-rate in a continuous manner (See Figure 3).

For improved stability of the numerical calculations it is advantageous (Reference 35) to write the right side of the energy equation, (A-3), in an alternate form. First note that*

$$\mu(I, p, D)\, D^2 = \frac{1}{2}\, \bar{\bar{V}} : \bar{\bar{D}}, \tag{A-7}$$

where $\bar{\bar{D}}$ is the deformation tensor and $\bar{\bar{V}}$ is the viscous-stress tensor. Upon using the identity

$$\operatorname{div}(\bar{\bar{V}} \cdot \bar{u}) = (\operatorname{div} \bar{\bar{V}}) \cdot \bar{u} + \frac{1}{2}\, \bar{\bar{V}} : \bar{\bar{D}} \tag{A-8}$$

it follows that (A-4) may be written in the form

$$\rho\left(\frac{\partial I}{\partial t} + u\,\frac{\partial I}{\partial r} + v\,\frac{\partial I}{\partial z}\right) + p \operatorname{div} \bar{u} = \operatorname{div}(\bar{\bar{V}} \cdot \bar{u}) - (\operatorname{div} \bar{\bar{V}}) \cdot \bar{u}. \tag{A-9}$$

If the right side is expanded some of the terms cancel and one obtains

$$\rho\left(\frac{\partial I}{\partial t} + u\,\frac{\partial I}{\partial r} + v\,\frac{\partial I}{\partial z}\right) + p \operatorname{div} \bar{u} =$$

$$\frac{\partial}{\partial r}\left[uV_{rr} + vV_{rz}\right] + \frac{\partial}{\partial z}\left[uV_{rz} + vV_{zz}\right]$$

$$- u\left[\frac{\partial V_{rr}}{\partial r} + \frac{\partial V_{rz}}{\partial z} - \frac{V_{\theta\theta}}{r}\right] - v\left[\frac{\partial V_{rz}}{\partial r} + \frac{\partial V_{zz}}{\partial z}\right], \tag{A-10}$$

*In Reference 6, $\bar{\bar{V}}$ and $\bar{\bar{D}}$ were denoted by τ^*_{ik} and D_{ik} respectively. In Reference 37 the latter quantity is denoted by $2\bar{\bar{D}}$.

where the components of the viscous stress tensor are given by

$$\begin{cases} V_{rr} = \mu\,(D_{rr} - \frac{2}{3}\,\mathrm{div}\,\bar{u}) = \mu\,(2\,\frac{\partial u}{\partial r} - \frac{2}{3}\,\mathrm{div}\,\bar{u}) \\ V_{\theta\theta} = \mu\,(D_{\theta\theta} - \frac{2}{3}\,\mathrm{div}\,\bar{u}) = \mu\,(2\,\frac{u}{r} - \frac{2}{3}\,\mathrm{div}\,\bar{u}) \\ V_{zz} = \mu\,(D_{zz} - \frac{2}{3}\,\mathrm{div}\,\bar{u}) = \mu\,(2\,\frac{\partial v}{\partial z} - \frac{2}{3}\,\mathrm{div}\,\bar{u}) \\ V_{rz} = \mu\,D_{rz} = \mu(\frac{\partial u}{\partial z} + \frac{\partial v}{\partial r}). \end{cases} \qquad \text{(A-11)}$$

The normal components of $\bar{\bar{V}}$ are the deviatoric stresses and $V_{rr} + V_{\theta\theta} + V_{zz} = 0$.

APPENDIX B

Consider a particle in cell $\binom{j}{i}$. During the (n + 1) th time cycle it may remain in that cell or it may move into one of the nearby cells. The particle would necessarily remain within its current cell or move into one of the eight nearest neighbor cells if δt were restricted to satisfy the inequalities.

$$\delta t \; u_{max} < h \qquad \delta t \; v_{max} < k. \tag{B-1}$$

The area averaging procedure described below does not require this restriction, and it has been found advantageous to relax the condition to permit (B-1) to be violated by several particles at each step. This permits δt to be chosen larger and greatly reduces the computation time with insignificant loss of accuracy.

Imagine a rectangle of cell size located about each particle, the particle being at the center (see sketch). The effective velocity for moving the particle is taken as the weighted average of the four cellwise velocities of the cell that the superposed rectangle overlaps. The weightings are proportional to the overlap areas.

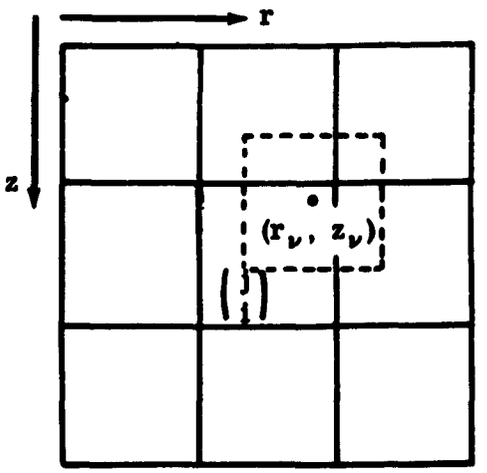

Consider, for example, the ν-th particle and suppose it is currently located in cell $\binom{j}{i}$. The appropriate values of i and j as well as the current coordinates of the particle, (r_ν, z_ν), are available at the end of Substep $\nu.2$ (see Table VI). Now the cells which the superposed rectangle overlaps vary

with the quadrant of cell $\binom{j}{i}$ within which the particle lies. Each possibility and its corresponding tentative new cellwise velocity, $\bar{\mathfrak{u}}_\nu = (\bar{u}_\nu, \bar{v}_\nu)$, are described in the following:

First Quadrant

$$\left.\begin{array}{l} (i-1/2)h \leq r_\nu < i\,h \\ (j-1)k \leq z_\nu < (j-1/2)k \end{array}\right\}$$

$$\bar{\mathfrak{u}}_\nu = \frac{1}{hk}\left\{\left[(j-1/2)k - z_\nu\right]\left(\left[r_\nu - (i-1/2)h\right]\bar{\mathfrak{u}}_{i+1}^{j-1} + \left[(i+1/2)h - r_\nu\right]\bar{\mathfrak{u}}_i^{j-1}\right)\right.$$
$$\left. + \left[z_\nu - (j-3/2)k\right]\left(\left[(i+1/2)h - r_\nu\right]\bar{\mathfrak{u}}_i^{j} + \left[r_\nu - (i-1/2)h\right]\bar{\mathfrak{u}}_{i+1}^{j}\right)\right\} \qquad \text{(B-2)}$$

If one of the overlapped cells is empty special provisions are required in using (B-2):

If $M_{i-1}^{j-1} = 0$ then set

$$\bar{u}_{i+1}^{j-1} = \bar{u}_i^j \qquad \bar{v}_{i+1}^{j-1} = \bar{v}_i^j.$$

If $M_i^{j-1} = 0$ then set

$$\bar{u}_i^{j-1} = \bar{u}_i^j \qquad \bar{v}_i^{j-1} = \bar{v}_i^j.$$

If $M_{i+1}^{j} = 0$ then set

$$\bar{u}_{i+1}^{j} = \bar{u}_i^j \qquad \bar{v}_{i+1}^{j} = \bar{v}_i^j.$$

If cell $\binom{j}{i}$ is adjacent to the right boundary of the mesh, $i = \beta$ and $j = 0, 1, \ldots, \gamma + 1$, then use (B-2) only set

$$\tilde{u}^{j-1}_{\beta+1} = \tilde{u}^{j-1}_{\beta} \qquad \tilde{v}^{j-1}_{\beta+1} = \tilde{v}^{j-1}_{\beta}$$

$$\tilde{u}^{j}_{\beta+1} = \tilde{u}^{j}_{\beta} \qquad \tilde{v}^{j}_{\beta+1} = \tilde{v}^{j}_{\beta} \ .$$

If cell $\binom{j}{i}$ is adjacent to the top boundary of the mesh, $j = 1$ and $i = 0, 1, \ldots, \beta + 1$, then use (B-2) only set

$$\tilde{u}^{0}_{i+1} = \tilde{u}^{1}_{i+1} \qquad \tilde{v}^{0}_{i+1} = \tilde{v}^{1}_{i+1}$$

$$\tilde{u}^{0}_{i} = \tilde{u}^{1}_{i} \qquad \tilde{v}^{0}_{i} = \tilde{v}^{1}_{i} \ .$$

Second Quadrant

$$\tilde{\bar{u}}_{\nu} = \frac{1}{hk}\Bigg\{\Big[(j - 1/2)k - z_{\nu}\Big]\Big(\Big[r_{\nu} - (i - 3/2)h\Big]\,\bar{u}^{j-1}_{i} + \Big[(i-1/2)h - r_{\nu}\Big]\,\bar{u}^{j-1}_{i-1}\Big) + \Big[z_{\nu} - (j - 3/2)k\Big]\Big(\Big[(i - 1/2)h - r_{\nu}\Big]\,\bar{u}^{j}_{i-1} + \Big[r_{\nu} - (i - 3/2)h\Big]\,\bar{u}^{j}_{i}\Big)\Bigg\} \qquad (B\text{-}3)$$

$$\left\{\begin{array}{l}(i - 1)h \leq r_{\nu} < (i - 1/2)h \\ (j - 1)k \leq z_{\nu} < (j - 1/2)k\end{array}\right\}$$

If one of the overlapped cells is empty special provisions are required in using (B-3):

If $M^{j-1}_{i} = 0$ then set

$$\tilde{u}^{j-1}_{i} = \tilde{u}^{j}_{i} \qquad \tilde{v}^{j-1}_{i} = \tilde{v}^{j}_{i}.$$

If $M_{i-1}^{j-1} = 0$ then set

$$\bar{u}_{i-1}^{j-1} = \bar{u}_i^j \qquad \bar{v}_{i-1}^{j-1} = \bar{v}_i^j .$$

If $M_{i-1}^{j} = 0$ then set

$$\bar{u}_{i-1}^{j} = \bar{u}_i^j \qquad \bar{v}_{i-1}^{j} = \bar{v}_i^j .$$

If cell $\binom{j}{i}$ is adjacent to the top boundary of the mesh, $j = 1$ and $i = 0, 1, \ldots, \beta + 1$, then in using (B-3) set

$$\bar{u}_i^0 = \bar{u}_i^1 \qquad \bar{v}_i^0 = \bar{v}_i^1$$

$$\bar{u}_{i-1}^0 = \bar{u}_{i-1}^1 \qquad \bar{v}_{i-1}^0 = \bar{v}_{i-1}^1 .$$

If cell $\binom{j}{i}$ is adjacent to the axis of symmetry, $i = 1$ and $j = 0, 1, \ldots, \gamma + 1$, then in using (B-3) set

$$\bar{u}_0^{j-1} = -\bar{u}_1^{j-1} \qquad \bar{v}_0^{j-1} = \bar{v}_1^{j-1}$$

$$\bar{u}_0^{j} = -\bar{u}_1^{j} \qquad \bar{v}_0^{j} = \bar{v}_1^{j}$$

Third Quadrant

$$\left.\begin{array}{l}(i-1)h \leq r_\nu < (i-1/2)h \\ (j-1/2)k \leq z_\nu < jk\end{array}\right\}$$

$$\tilde{\tilde{u}}_\nu = \frac{1}{hk}\left\{\left[(j+1/2)k - z_\nu\right]\left(\left[r_\nu - (i-3/2)h\right]\tilde{\tilde{u}}_i^j + \left[(i-1/2)h - r_\nu\right]\tilde{\tilde{u}}_{i-1}^j\right)\right.$$
$$\left. + \left[z_\nu - (j-1/2)k\right]\left(\left[(i-1/2)h - r_\nu\right]\tilde{\tilde{u}}_{i-1}^{j+1} + \left[r_\nu - (i-3/2)h\right]\tilde{\tilde{u}}_i^{j+1}\right)\right\} \quad \text{(B-4)}$$

If one of the overlapped cells is empty special provisions are required in using (B-4):

If $M_{l-1}^j = 0$ then set

$$\tilde{u}_{i-1}^j = \tilde{u}_i^j \qquad \tilde{v}_{i-1}^j = \tilde{v}_i^j.$$

If $M_{i-1}^{j+1} = 0$ then set

$$\tilde{u}_{i-1}^{j+1} = \tilde{u}_i^j \qquad \tilde{v}_{i-1}^{j+1} = \tilde{v}_i^j.$$

If $M_i^{j+1} = 0$ then set

$$\tilde{u}_i^{j+1} = \tilde{u}_i^j \qquad \tilde{v}_i^{j+1} = \tilde{v}_i^j.$$

If cell $\begin{pmatrix} j \\ i \end{pmatrix}$ is adjacent to the axis of symmetry, $i = 1$ and $j = 0, 1, \ldots, \gamma + 1$, then in using (B-4) set

$$u_0^j = -u_1^j \qquad v_0^j = v_1^j$$

$$u_0^{j+1} = -u_1^{j+1} \qquad v_0^{j+1} = v_1^{j+1} .$$

If cell $\begin{pmatrix} j \\ i \end{pmatrix}$ is adjacent to the bottom boundary of the mesh, $j = \gamma$ and $i = 0, 1, \ldots, \beta + 1$, then in using (B-4) set

$$\underset{\sim}{u}_{i-1}^{\gamma+1} = \underset{\sim}{u}_{i-1}^{\gamma} \qquad \underset{\sim}{v}_{i-1}^{\gamma+1} = \underset{\sim}{v}_{i-1}^{\gamma}$$

$$\underset{\sim}{u}_{i}^{\gamma+1} = \underset{\sim}{u}_{i}^{\gamma} \qquad \underset{\sim}{v}_{i}^{\gamma+1} = \underset{\sim}{v}_{i}^{\gamma} .$$

Fourth Quadrant

$$\left\{ \begin{array}{l} (i - 1/2)h \leq r_\nu < ih \\ (j - 1/2)k \leq z_\nu < jk \end{array} \right\}$$

$$\underset{\sim}{u}_\nu = \frac{1}{hk} \left\{ \left[(j + 1/2)k - z_\nu \right] \left(\left[r_\nu - (i - 1/2)h \right] \underset{\sim}{u}_{i+1}^{j} + \left[(i + 1/2)h - r_\nu \right] \underset{\sim}{u}_{i}^{j} \right) \right.$$

$$\left. + \left[z_\nu - (j - 1/2)k \right] \left(\left[(i + 1/2)h - r_\nu \right] \underset{\sim}{u}_{i}^{j+1} + \left[r_\nu - (i - 1/2)h \right] \underset{\sim}{u}_{i+1}^{j+1} \right) \right\} \qquad \text{(B-5)}$$

If one of the overlapped cells is empty special provisions are required in using (B-5):

If $M_{i+1}^j = 0$ then set

$$\underset{\sim}{u}_{i+1}^{j} = \underset{\sim}{u}_{i}^{j} \qquad \underset{\sim}{v}_{i+1}^{j} = \underset{\sim}{v}_{i}^{j} .$$

If $M_i^{j+1} = 0$ then set

$$\tilde{u}_i^{j+1} = \tilde{u}_i^j \qquad \tilde{v}_i^{j+1} = \tilde{v}_i^j.$$

If $M_{i+1}^{j+1} = 0$ then set

$$\tilde{u}_{i+1}^{j+1} = \tilde{u}_i^j \qquad \tilde{v}_{i+1}^{j+1} = \tilde{v}_i^j.$$

If cell $\binom{j}{i}$ is adjacent to the bottom boundary of the mesh, $j = \gamma$ and $i = 0, 1, \ldots, \beta + 1$, then in using (B-5) set

$$\tilde{u}_i^{\gamma+1} = \tilde{u}_i^{\gamma} \qquad \tilde{v}_i^{\gamma+1} = \tilde{v}_i^{\gamma}$$

$$\tilde{u}_{i+1}^{\gamma+1} = \tilde{u}_{i+1}^{\gamma} \qquad \tilde{v}_{i+1}^{\gamma+1} = \tilde{v}_{i+1}^{\gamma}.$$

If cell $\binom{j}{i}$ is adjacent to the right boundary of the mesh, $i = \beta$ and $j = 0, 1 \ldots, \gamma + 1$, then in using (B-5) set

$$\tilde{u}_{\beta+1}^{j} = \tilde{u}_{\beta}^{j} \qquad \tilde{v}_{\beta+1}^{j} = \tilde{v}_{\beta}^{j}$$

$$\tilde{u}_{\beta+1}^{j+1} = \tilde{u}_{\beta}^{j+1} \qquad \tilde{v}_{\beta+1}^{j+1} = \tilde{v}_{\beta}^{j}.$$

APPENDIX C

In the computational procedure the normal and shearing stresses along each continuative boundary are assigned to be just equal to their corresponding values in the adjacent interior cell. Surface forces are thereby assigned to the mesh once the disturbances produced by the impact are propagated to the mesh boundary. The momentum and energy produced by the surface loading must be accounted for if the conservation relations (83) and (84) are to remain valid throughout the computations. For each cell along a continuative boundary it is necessary to make the following additions to the energy and momentum cumulations:

Right Mesh Boundary (excluding corner cells):

$$i = \beta \text{ and } j = 2, 3, \ldots, \gamma - 1$$

$$\Delta^j_\beta (E'_s)^{\text{diff.}}_{\text{out}} = \left\{ \hat{u}^j_\beta \left[p^j_\beta - (V_{rr})^j_\beta \right] - \hat{v}^j_\beta (V_{rz})^j_\beta \right\} \left[2\pi \beta hk \delta t \right]$$

$$\Delta^j_\beta (R'_s)^{\text{diff}}_{\text{out}} = - P^j_\beta \left[2\pi \beta hk \delta t \right]$$

$$\Delta^j_\beta (Z'_s)^{\text{diff}}_{\text{out}} = - Q^j_\beta \left[2\pi \beta hk \delta t \right]$$

Bottom Mesh Boundary (excluding right corner cell):

$$j = \gamma \text{ and } i = 1, 2, \ldots, \beta - 1$$

$$\Delta^\gamma_i (E'_s)^{\text{diff}}_{\text{out}} = \left\{ \hat{v}^\gamma_i \left[p^\gamma_i - (V_{zz})^\gamma_i \right] - \hat{u}^\gamma_i (V_{rz})^\gamma_i \right\} \left[2\pi (i-1/2)\, h^2 \delta t \right]$$

$$\Delta^\gamma_i (R'_s)^{\text{diff}}_{\text{out}} = -Q^\gamma_i \left[2\pi (i-1/2)\, h^2 \delta t \right]$$

$$\Delta^\gamma_i (Z'_s)^{\text{diff}}_{\text{out}} = - P^\gamma_i \left[2\pi (i-1/2)\, h^2 \delta t \right]$$

Top Mesh Boundary (excluding right corner cell):

$$j = 1 \text{ and } i = 1, 2, \ldots, \beta - 1$$

$$\Delta_i^1 (E'_s)_{out}^{diff} = \left\{ -\hat{v}_i^1 \left[p_i^1 - (V_{zz})_i^1 \right] + \hat{u}_i^1 (V_{rz})_i^1 \right\} \left[2\pi(i-1/2)\ h^2\ \delta t \right]$$

$$\Delta_i^1 (R'_s)_{out}^{diff} = Q_i^1 \left[2\pi(i-1/2)\ h^2 \delta t \right]$$

$$\Delta_i^1 (Z'_s)_{out}^{diff} = P_i^1 \left[2\pi(i-1/2)\ h^2 \delta t \right]$$

Lower Right Mesh Corner, $i = \beta$ and $j = \gamma$:

$$\Delta_\beta^\gamma (E'_s)_{out}^{diff} = \left\{ \hat{u}_\beta^\gamma \left[p_\beta^\gamma - (V_{rr})_\beta^\gamma \right] - \hat{v}_\beta^\gamma (V_{rz})_\beta^\gamma \right\} \left[2\pi\ \beta hk\, \delta t \right]$$
$$+ \left\{ \hat{v}_\beta^\gamma \left[p_\beta^\gamma - (V_{zz})_\beta^\gamma \right] - \hat{u}_\beta^\gamma (V_{rz})_\beta^\gamma \right\} \left[2\pi(\beta-1/2)\ h^2 \delta t \right]$$

$$\Delta_\beta^\gamma (R'_s)_{out}^{diff} = -P_\beta^\gamma \left[2\pi\ \beta hk\, \delta t \right] - Q_\beta^\gamma \left[2\pi(\beta-1/2)\ h^2 \delta t \right]$$

$$\Delta_\beta^\gamma (Z'_s)_{out}^{diff} = -Q_\beta^\gamma \left[2\pi\ \beta hk\, \delta t \right] - P_\beta^\gamma \left[2\pi(\beta-1/2)\ h^2 \delta t \right]$$

Upper Right Mesh Corner, $i = \beta$ and $j = 1$:

$$\Delta_\beta^1 (E'_s)_{out}^{diff} = \left\{ \hat{u}_\beta^1 \left[p_\beta^1 - (V_{rr})_\beta^1 \right] - \hat{v}_\beta^1 (V_{rz})_\beta^1 \right\} \left[2\pi\beta hk\ \delta t \right]$$
$$+ \left\{ \hat{u}_\beta^1 (V_{rz})_\beta^1 - \hat{v}_\beta^1 \left[p_\beta^1 - (V_{zz})_\beta^1 \right] \right\} \left[2\pi(\beta-1/2)\ h^2 \delta t \right]$$

$$\Delta_\beta^1 (R'_s)_{out}^{diff} = -P_\beta^1 \left[2\pi\beta hk\ \delta t \right] + Q_\beta^1 \left[2\pi(\beta-1/2)\ h^2 \delta t \right]$$

$$\Delta_\beta^1 (Z'_s)_{out}^{diff} = -Q_\beta^1 \left[2\pi\beta hk \delta t \right] + P_\beta^1 \left[2\pi(\beta-1/2)\ h^2 \delta t \right]$$

TABLE I

Viscosity parameters, defined by equations (7) and (8), expressed in the gm-cm-μsec system of units are given. c is a mean value for the specific heat and η (0, 0) is the extrapolated value of $\eta(I,p)$ at $I = p = 0$. These should be considered only as zero-order approximations in the hypervelocity regime.

Metal	$A \times 10^{11}$	$C \times 10^{-2}$	$\eta(0,0)$	$c \times 10^{6}$	$\mu_o \times 10^{11}$	$\mu_1 \times 10^{3}$	$\mu_2 \times 10^{4}$
Tin	465.	7.29	5.28×10^{-8}	2.72	465	1.98	8.16
Cadmium	540.	9.32	12.1×10^{-8}	2.76	540	2.57	8.27
Lead	424.	11.5	19.4×10^{-8}	1.42	424	1.63	4.26
Zinc	399.	15.0	59.2×10^{-8}	4.6	399	6.90	13.8
Copper	609.	24.4	2.07×10^{-5}	4.2	609	10.25	12.6
Aluminum	1.20	75.8	1.11	9.62	1.20	72.9	28.9
Steel							
Fe(97.5)-C(2.5)	10.4	85.7	261	6.07	10.4	52.0	18.2
Fe(97.0)-C(3.0)	10.9	87.4	475	6.07	10.9	53.0	18.2
Fe(97.5)-C(3.5)	9.2	90.5	1135	6.07	9.2	54.9	18.2

The values quoted here are taken from handbooks, References 11 and 12. A further source of information is Reference 13.

TABLE II

Equation of state parameters, occurring in relation (15), expressed in the gm-cm-μsec system of units.

	Aluminum	Iron
a_1	1.1867	7.78
a_2	0.76300	31.18
b_o	3.4448	9.591
b_1	1.5451	15.676
b_2	0.96430	4.634
c_o	0.43382	0.3984
c_1	0.54873	0.5306
ϕ_o	1.5000	9.00
ρ_o	2.702	7.86

$$\xi_1 = \xi_2 = 0 \text{ for } t < t^*$$

$$\xi_1 = \xi_2 = 0.045 \text{ for } t > t^*$$

Here t^* is the time after which a major signal has passed over the material.

TABLE III

Values of the material parameters required in the strength - time relation, equation (24) used to predict fracture (References 22 and 24).

Metal	$\lambda \times 10^{-4}$ (degrees)	$\omega \times 10^{-7}$ (degrees/mb)	t_o (μsec)
Aluminum (annealed at 550°C)	2.55	5.1	2.5×10^{-5}
Aluminum (annealed at 420°C)	2.5	3	2.5×10^{-5}
Zinc	1.25	0.8	6.6×10^{-3}*
Silver	3.2	0.9	3.55×10^{-8}*
Nickel	4.35	0.3	1.55×10^{-7}**
Platinum	6.25	3.85	7.9×10^{-7}

*Obtained from single σ vs log t curve at 18°C
**Estimated from formula

$$t_o \approx h\,(k\,\theta_D)^{-1}$$

where h is Planck's constant, k Boltzmann's constant and θ D is the Debye temperature (Reference 25).

TABLE IV

Sequence of cellwise storage changes for cell $\binom{j}{i}$ during phase I of the calculations.

Register No.	1	2	3	4	5	6	7	8	9	10	11	12	13	14
	M_i^j	I_i^j	u_i^j	v_i^j	p_i^j	—	—	—	—	—	—	—	—	—
STEP 1.1	"	"	"	"	"	$u_{i-1/2}^j$	$v_{i-1/2}^j$	$u_i^{j-1/2}$	$v_i^{j-1/2}$	—	—	—	—	—
STEP 1.2	"	"	"	"	"	"	"	"	"	$(\mathrm{div}\,\vec{u})_i^j$	—	—	—	—
STEP 1.3	"	"	"	"	"	"	"	"	"	"	$(D^2)_i^j$	—	—	—
STEP 1.4	"	"	"	"	"	μ_i^j	"	"	"	"	"	—	—	—
STEP 1.5	"	"	"	"	"	"	"	"	Q_i^j	P_i^j	"	$(r^2)_i^j$	—	—
STEP 1.6	"	"	"	"	"	"	$P_{i-1/2}^j$	$\left(\frac{u}{r}\right)_{i-1/2}^j$	"	"	$\mu_{i-1/2}^j$	$Q_i^{j-1/2}$	—	—
STEP 1.7	"	"	"	"	"	"	"	$\tilde{u}_i^j$	"	"	"	"	—	—

TABLE IV

(Continued)

	1	2	3	4	5	6	7	8	9	10	11	12	13	14
	M_i^j	I_i^j	u_i^j	v_i^j	p_i^j	μ_i^j	$P_{i-\frac{1}{2}}^j$	$\tilde{u}_i^j$	Q_i^j	P_i^j	$\mu_{i-1/2}^j$	$Q_i^{j-\frac{1}{2}}$	—	—
STEP 1.8	"	"	"	"	"	"	$P_i^{j-\frac{1}{2}}$	"	"	"	$\mu_i^{j-1/2}$	$(rQ)_{i-\frac{1}{2}}^j$	—	—
STEP 1.9	"	"	"	"	"	"	"	"	$\tilde{v}_i^j$	"	"	"	—	—
STEP 1.10	"	"	"	"	"	"	"	$\hat{u}_i^j$	$\hat{v}_i^j$	"	"	"	—	—
STEP 1.11	"	"	"	"	"	$\hat{u}_{i-1/2}^j$	$\hat{v}_{i-1/2}^j$	"	"	$\hat{u}_i^{j-1/2}$	$\hat{v}_i^{j-1/2}$	"	—	—
STEP 1.12	"	"	"	"	"	"	"	"	"	"	"	$(\mathrm{div}\,\hat{\vec{u}})_i^j$	—	—
STEP 1.13	"	"	"	"	"	"	"	"	"	"	"	"	Ψ_i^j	$\left(\hat{D}^2\right)_i^j$
STEP 1.14	"	"	"	"	"	"	"	"	"	"	"	"	"	$\hat{\mu}_i^j$

TABLE IV

(Continued)

	1	2	3	4	5	6	7	8	9	10	11	12	13	14
	M_i^j	I_i^j	u_i^j	v_i^j	p_i^j	$\hat{u}^j_{i-1/2}$	$\hat{v}^j_{i-1/2}$	$\hat{u}^j_i$	$\hat{v}^j_i$	$\hat{u}^{j-1/2}_i$	$\hat{v}^{j-1/2}_i$	$(\widehat{\text{div}\,\tilde{u}})^j_i$	Ψ^j_i	$\hat{\mu}^j_i$
STEP 1.15	"	"	"	"	"	$(V_{rr})^j_i$	"	"	"	$(V_{rz})^j_i$	$(V_{zz})^j_i$	"	"	"
STEP 1.16	"	"	"	"	"	"	$\Lambda^j_{i-1/2}$	"	"	"	"	"	"	$(V_{\theta\theta})^j_i$
STEP 1.17	"	"	"	"	$(V_{max})^j_i$	"	"	"	"	"	"	$\Omega^{j-1/2}_i$	Γ^j_i	"
STEP 1.18	"	"	"	"	"	"	"	"	"	"	$(V_{zz})^{j-1/2}_i$	"	"	$(V_{rz})^{j-1/2}_i$
STEP 1.19	"	"	"	"	"	$(V_{rr})^j_{i-1/2}$	"	"	"	$(V_{rz})^j_{i-1/2}$	"	"	"	"
STEP 1.20	"	$\tilde{I}^j_i$	"	"	"	"	"	"	"	"	"	"	"	"
STEP 1.21	"	"	"	"	"	"	"	$\tilde{u}^j_i$	$\tilde{v}^j_i$	"	"	"	"	"

TABLE V

Sequence of cellwise storage changes for cell $\binom{j}{i}$ during phase II of the calculations.

Register No.	1	2	3	4	5	6	7	8	9	10	11	12	13	14
	M_i^j	$\tilde{I}_i^j$	u_i^j	v_i^j	$(v_{max})_i^j$	$(v_{rr})_{i-\frac{1}{2}}^j$	$\Delta_{i-\frac{1}{2}}^j$	$\tilde{u}_i^j$	$\tilde{v}_i^j$	$(v_{rz})_{i-\frac{1}{2}}^j$	$(v_{zz})_i^{j-\frac{1}{2}}$	$\Omega_i^{j-1/2}$	Γ_i^j	$(v_{rz})_i^{j-\frac{1}{2}}$
STEP 2.1	"	"	"	"	"	$\tilde{R}_i^j$	$\tilde{Z}_i^j$	"	"	"	"	"	"	$\tilde{E}_i^j$
STEP 2.2	"	"	"	"	"	"	"	"	"	0	0	0	0	"
STEP 2.3	"	"	"	"	"	"	"	"	"	$M_i^{j'}$	$E_i^{j'}$	$R_i^{j'}$	$Z_i^{j'}$	"
STEP 2.4	$M_i^{j'}$	"	$u_i^{j'}$	$v_i^{j'}$	"	$\rho_i^{j'}$	"	"	"	"	"	"	"	"
STEP 2.5	"	$I_i^{j'}$	"	"	"	"	"	"	"	"	"	"	"	"
STEP 2.6	"	"	"	"	"	"	$\tilde{p}_i^j$	"	"	"	"	"	"	"
STEP 2.7	"	"	"	"	$p_i^{j'}$	"	"	"	"	"	"	"	"	"

TABLE VI

Schematic depicting of sequence of substeps associated with the motion of the ν-th particle during Step 2.3.

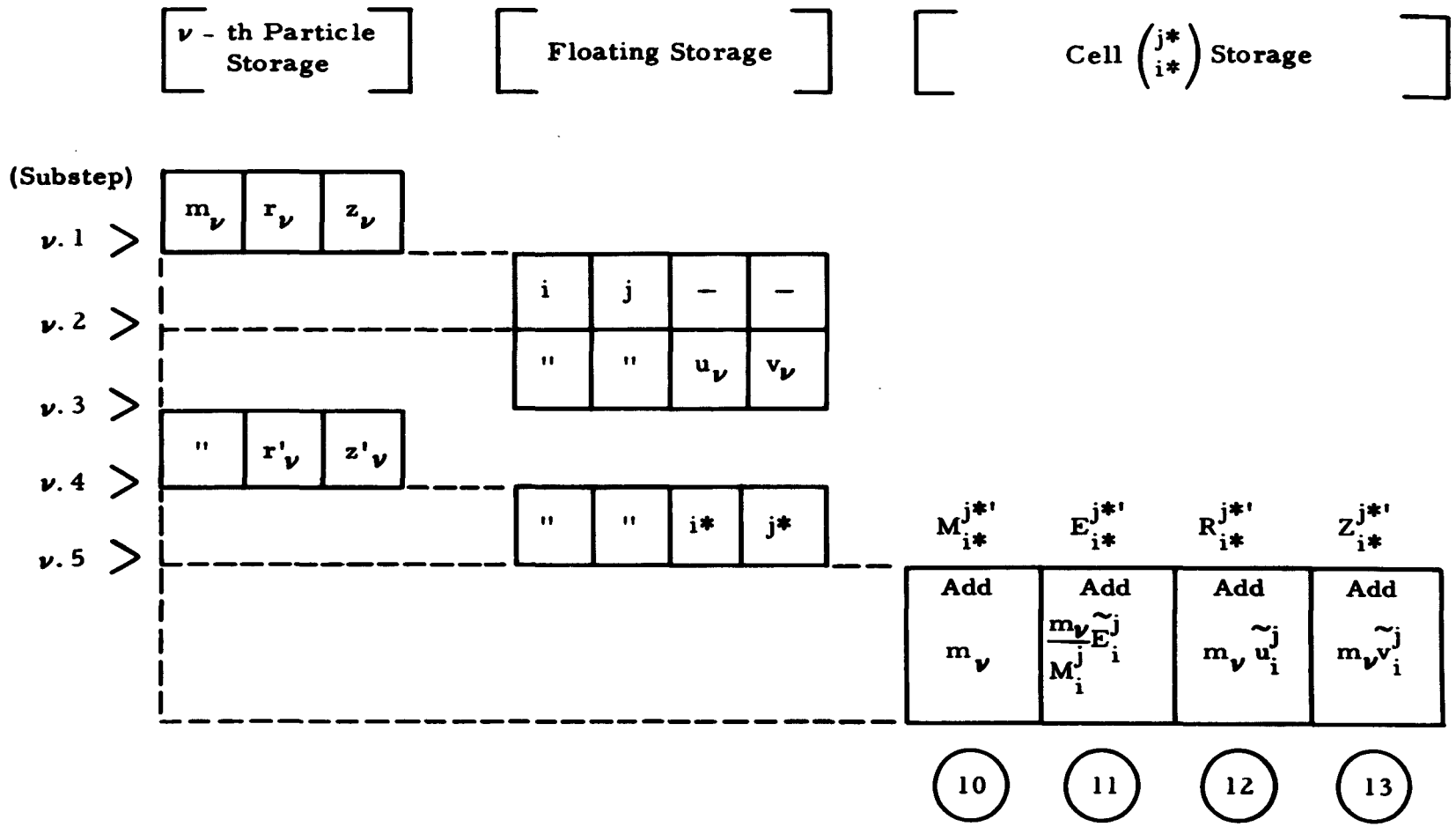

TABLE VII

Schematic of the cumulation processes for the phase III calculations associated with the projectile-target system.

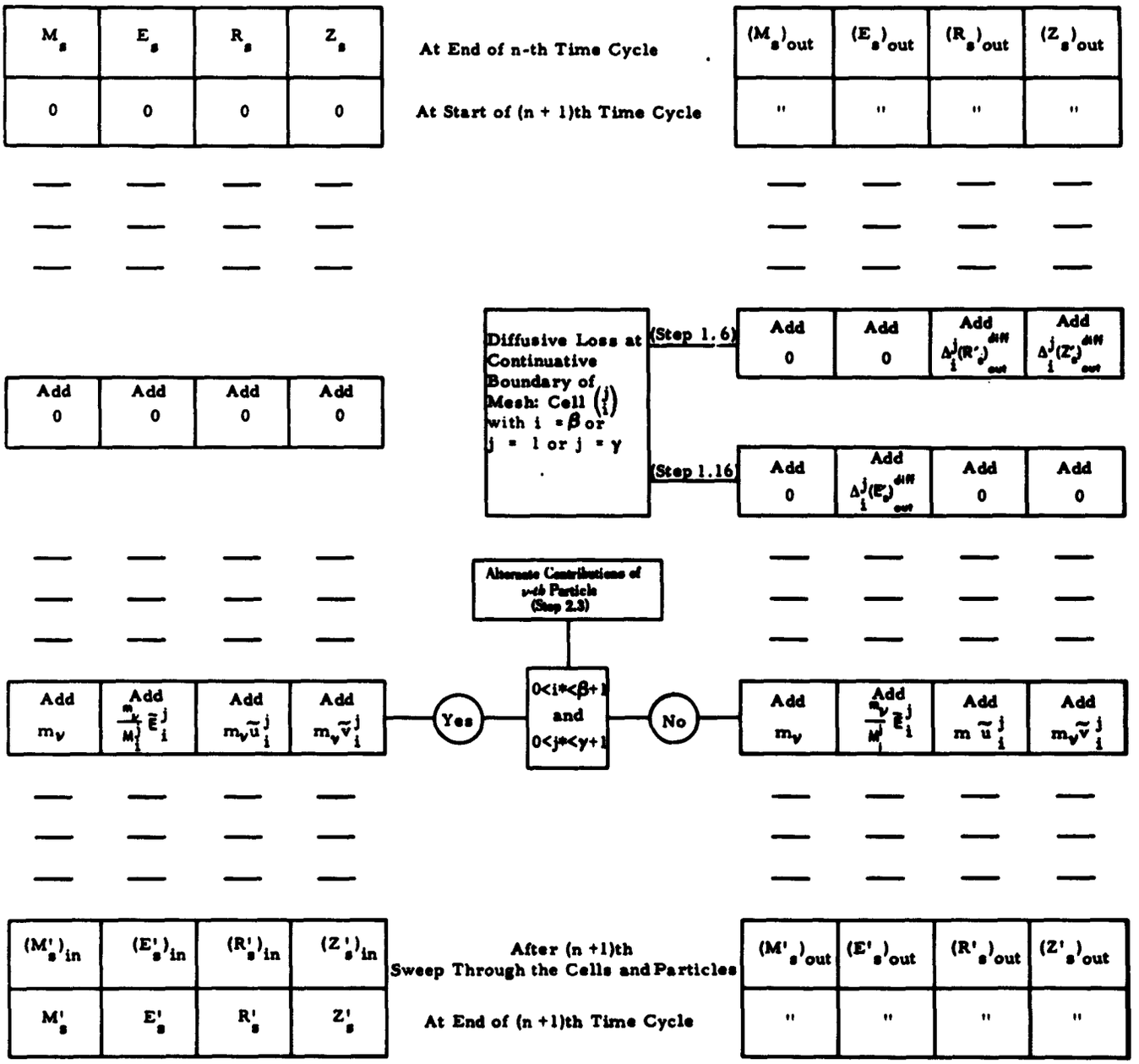

TABLE VIII

Schematic of the accumulation process for the phase III calculations associated with the projectile material

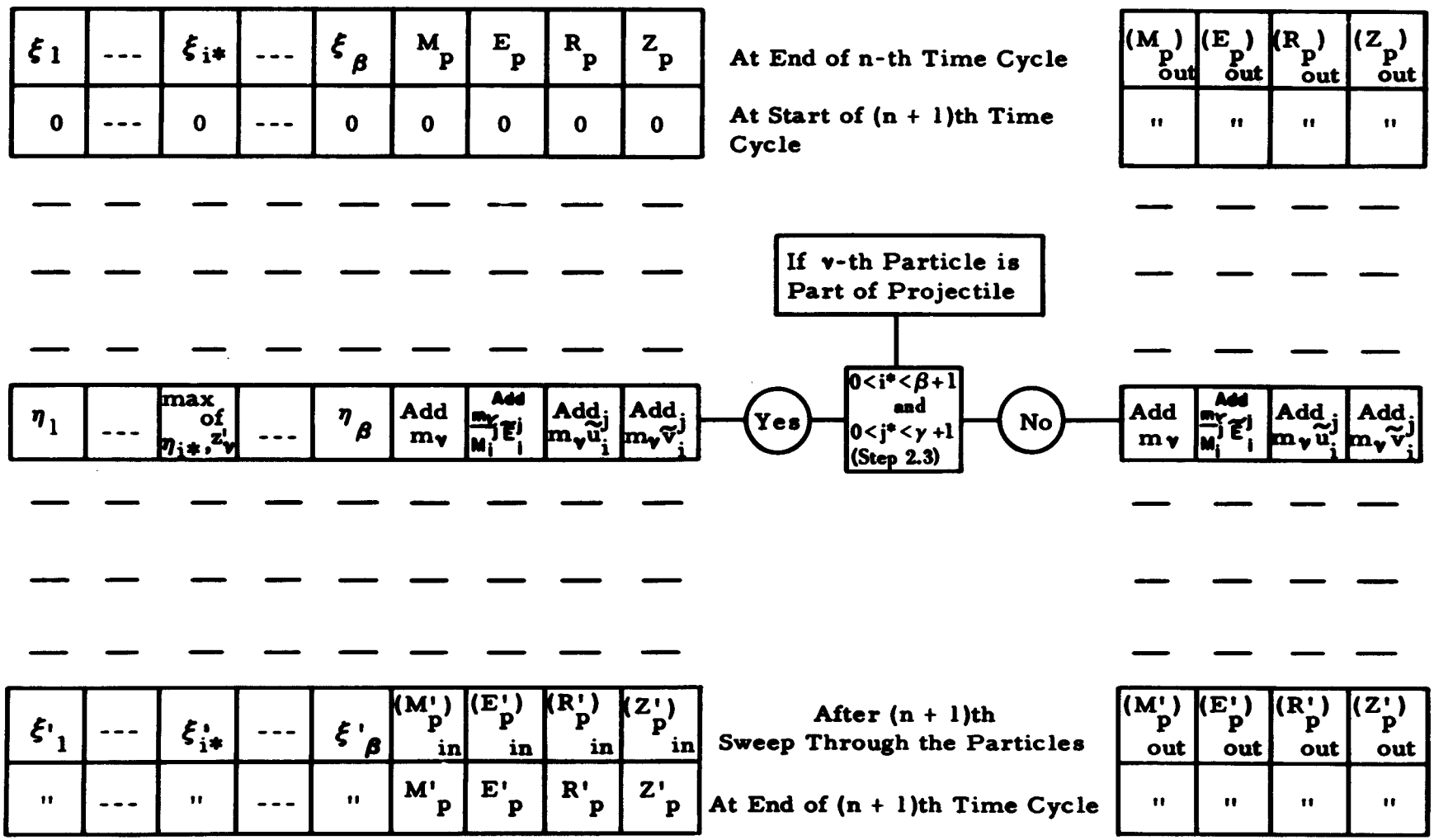

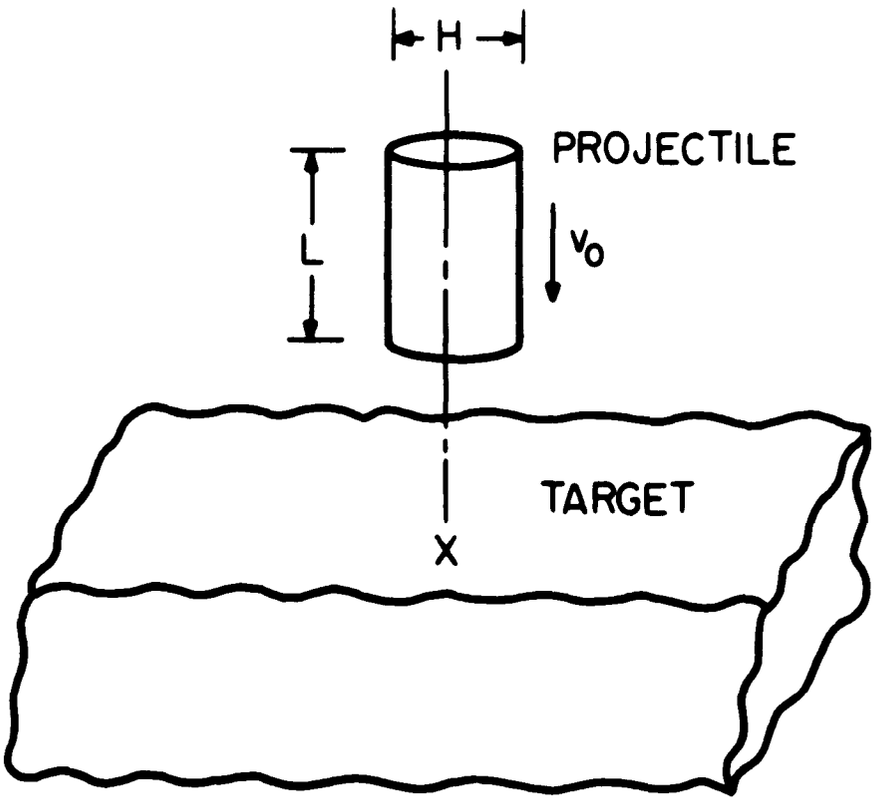

Figure 1. Illustration of projectile-target configuration just before impact.

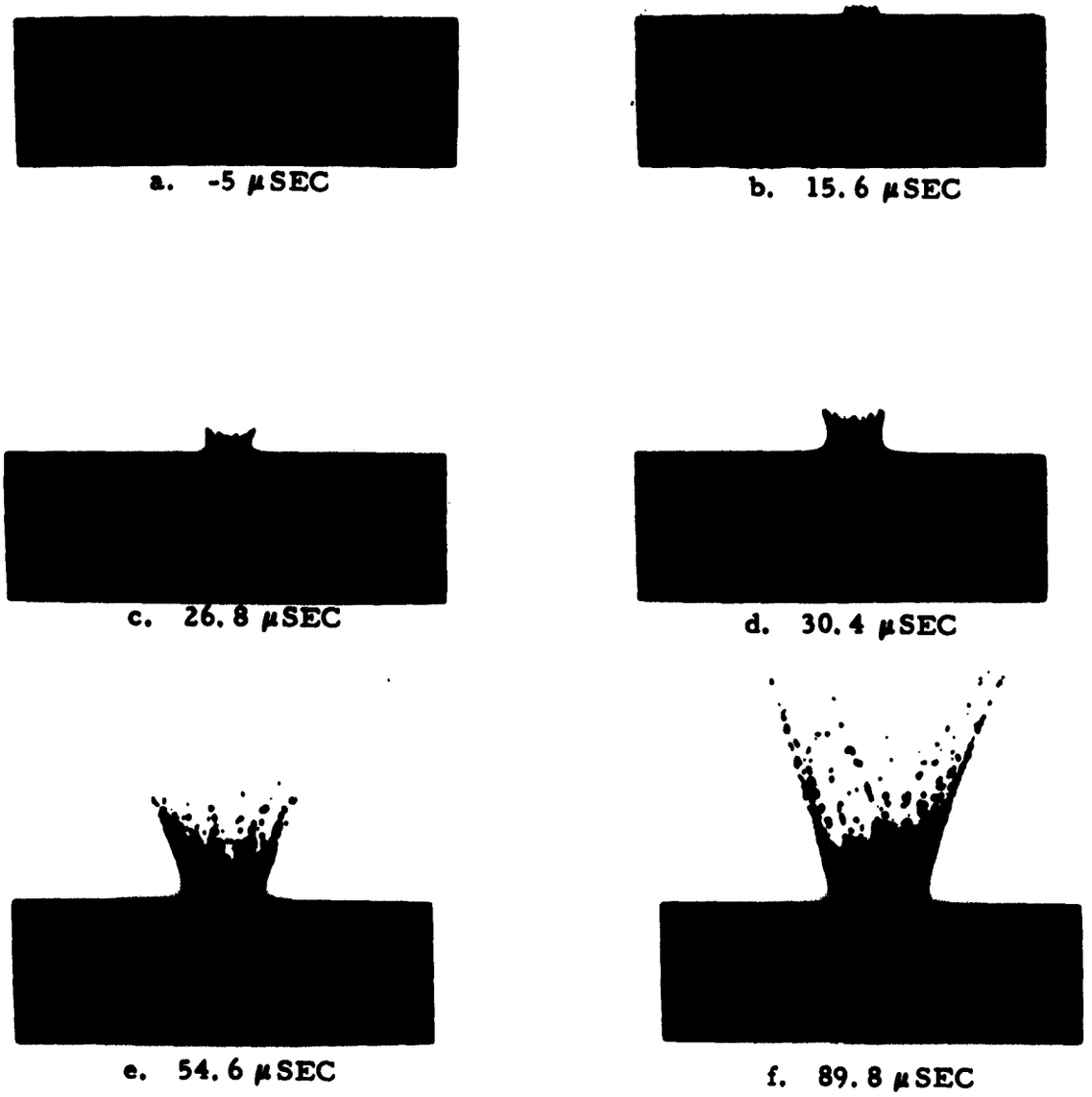

Figure 2. Illustration of violent ejection of material from target during the formation of a crater. In (a) the projectile-target system is depicted just prior to impact; the subsequent ejection is depicted in the sequence (b) to (e). (Sketched from photographs obtained at BRL)

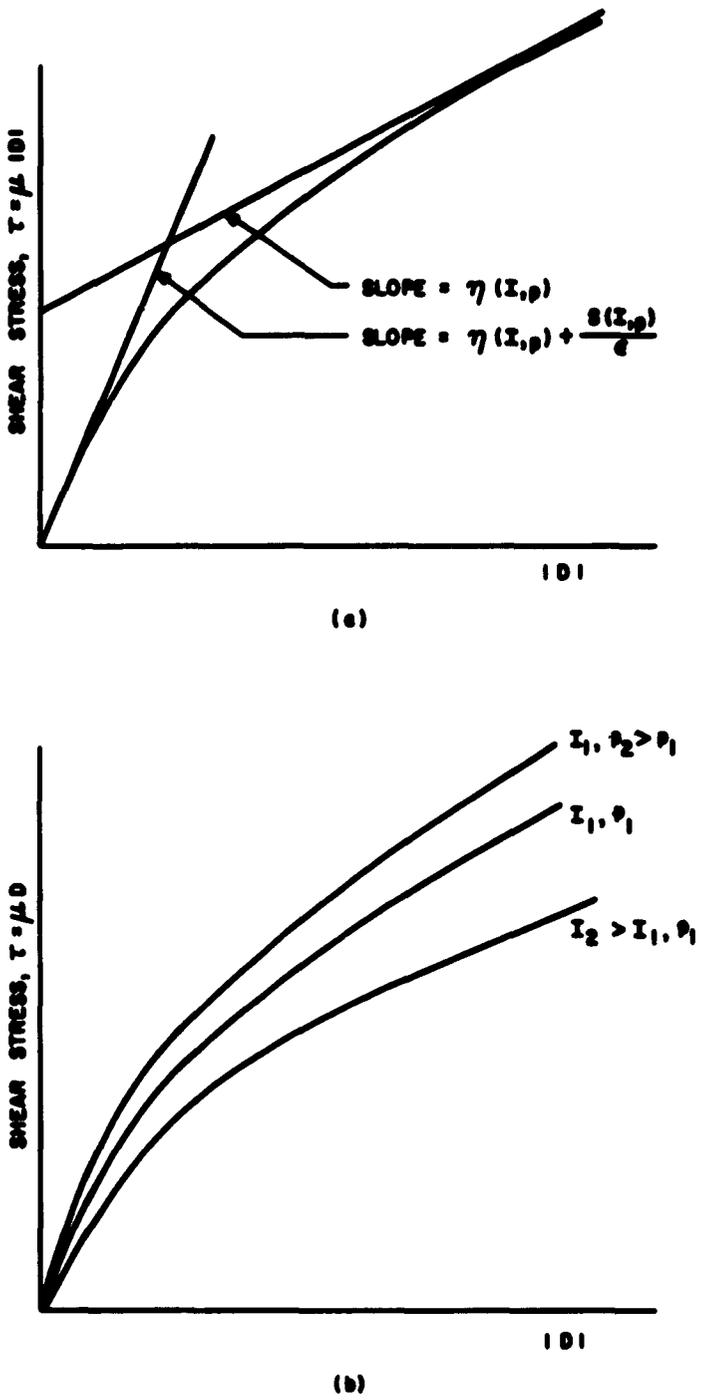

Figure 3. Schematic representing the dependence of the shearing stress on the rate of deformation: (a) Effect of ϵ, (b) Effect of internal energy (or temperature) and pressure.

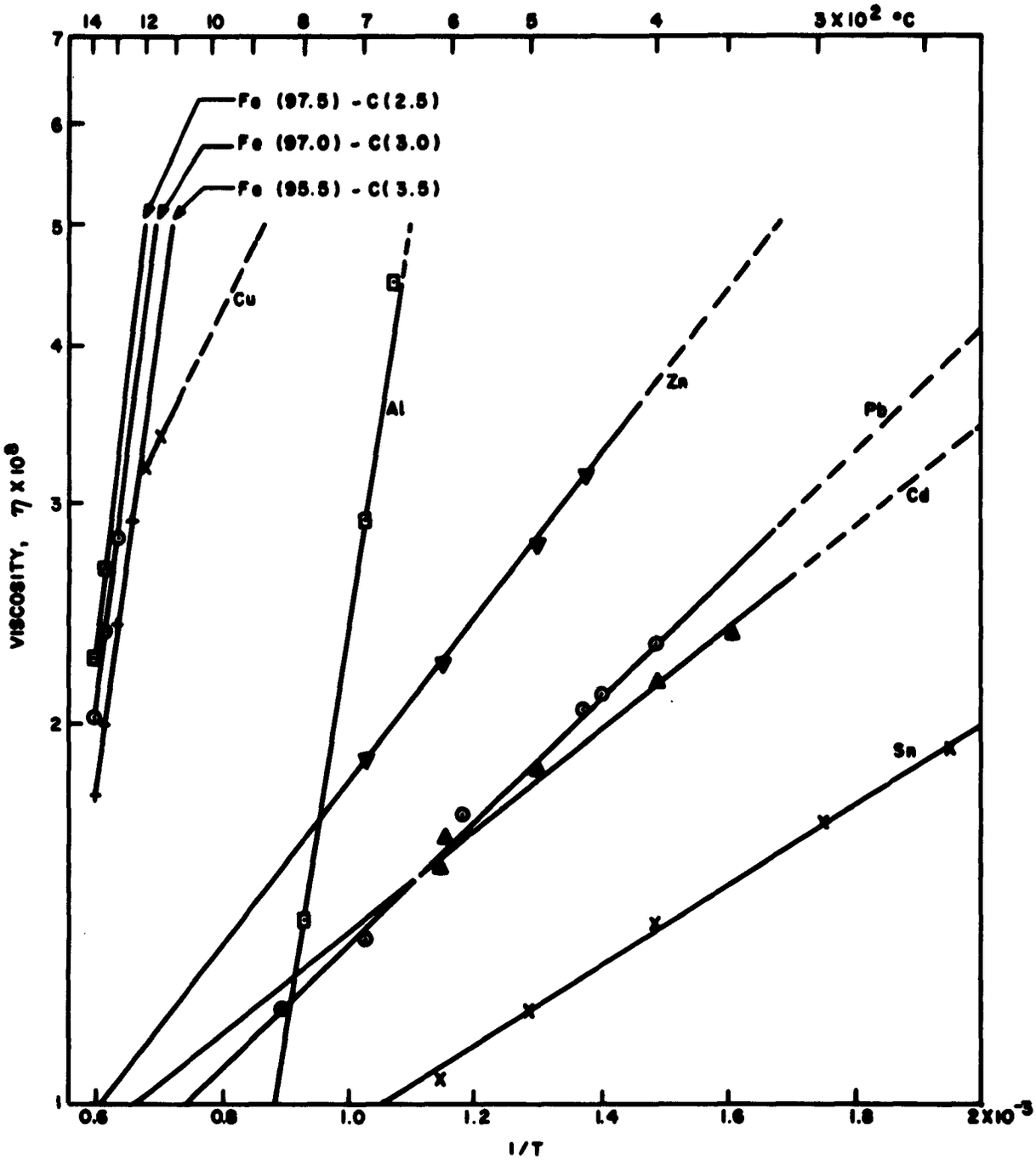

Figure 4. Viscosity factor depicted as a function of the inverse of the absolute temperature. η is given in the gm-cm-μsec system of units (from References 11 and 12). The curves are broken for temperatures in the solid phase range.

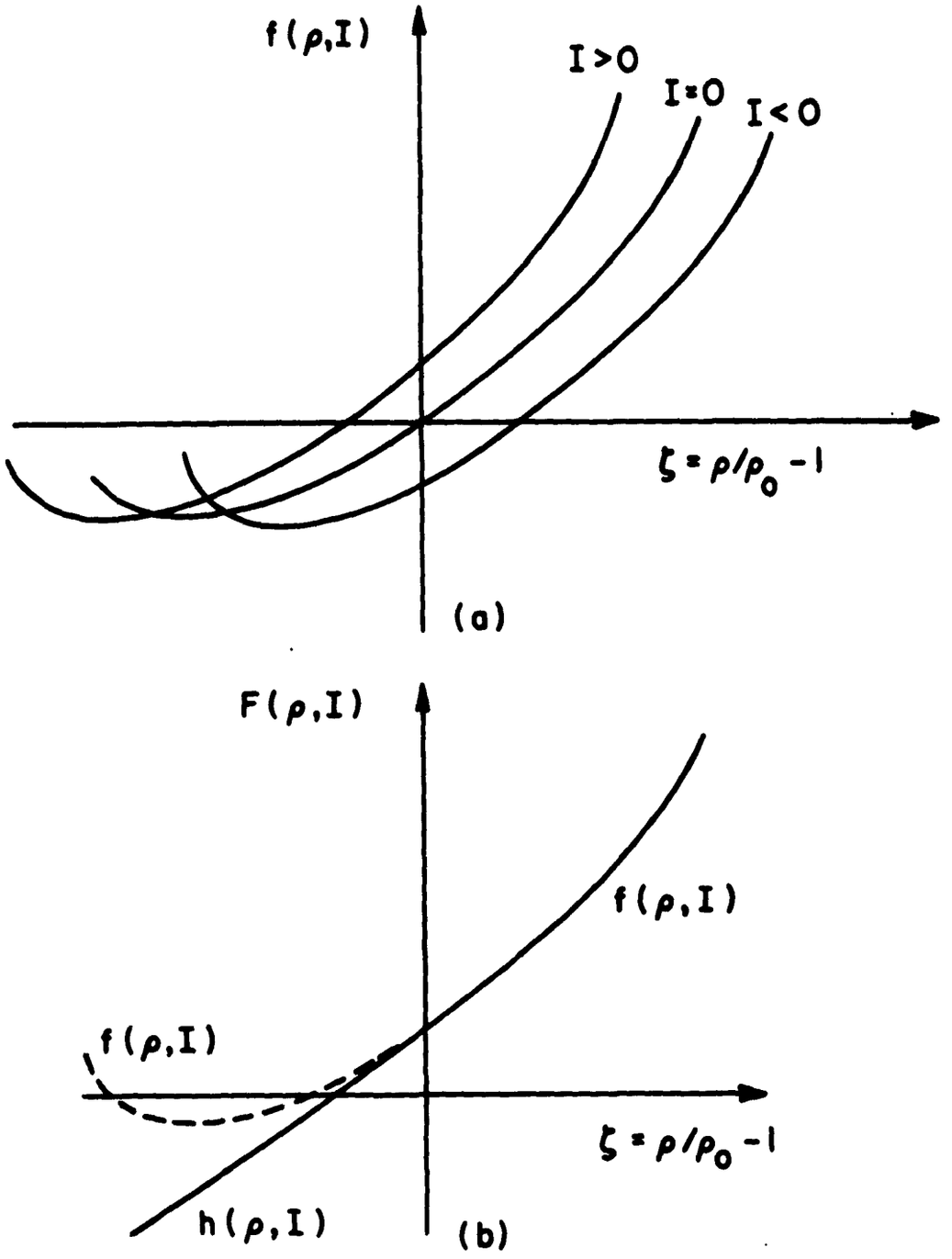

Figure 5. Schematic of equation of state:
(a) Function equal to pressure in compressive region.
(b) Extrapolation into tensile region.

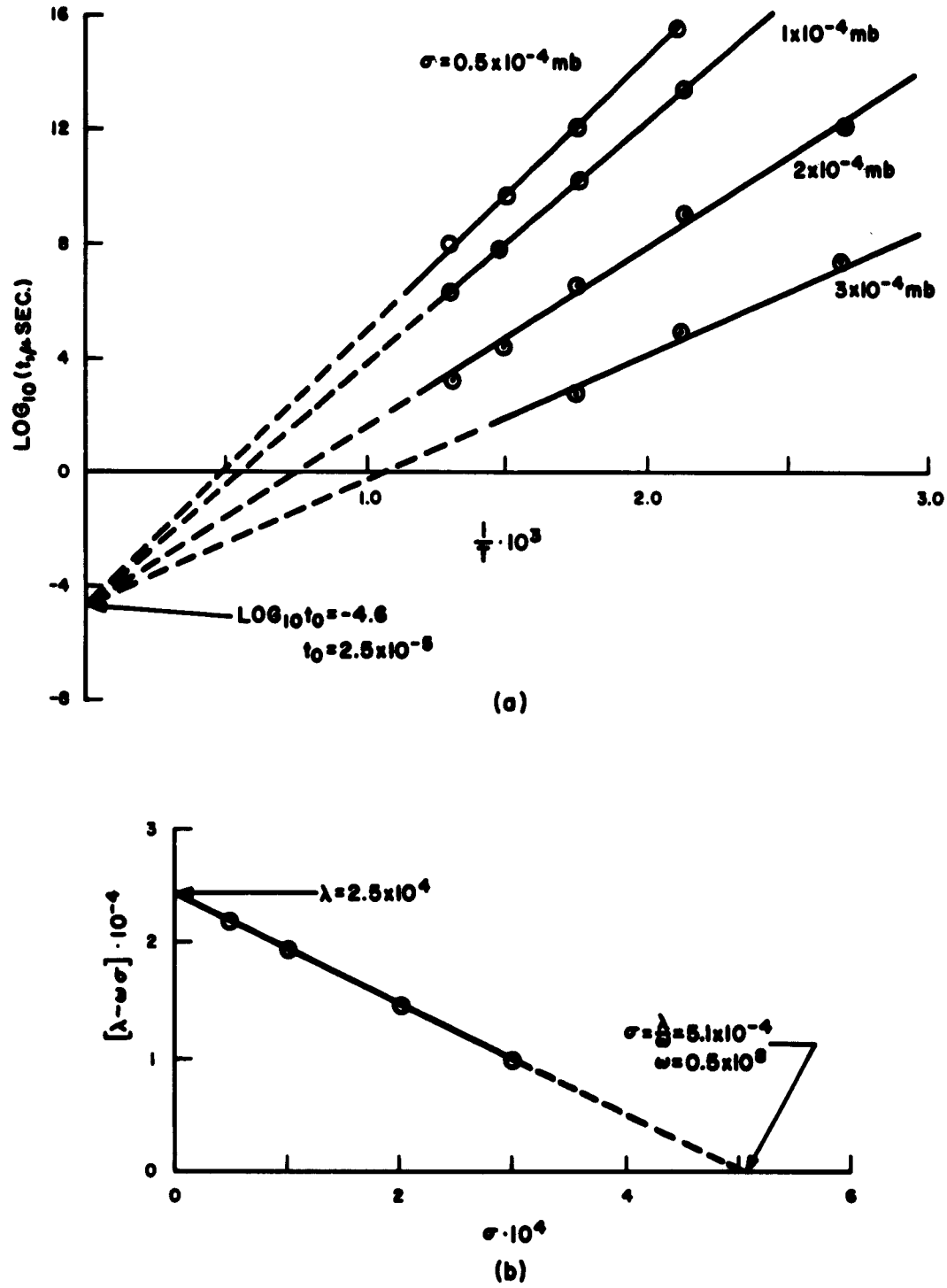

Figure 6. Strength-time-temperature behavior of platinum (References 22 and 24): (a) Dependence of time to fracture on the absolute temperature (b) Dependence of $\lambda - \omega\sigma$ on σ.

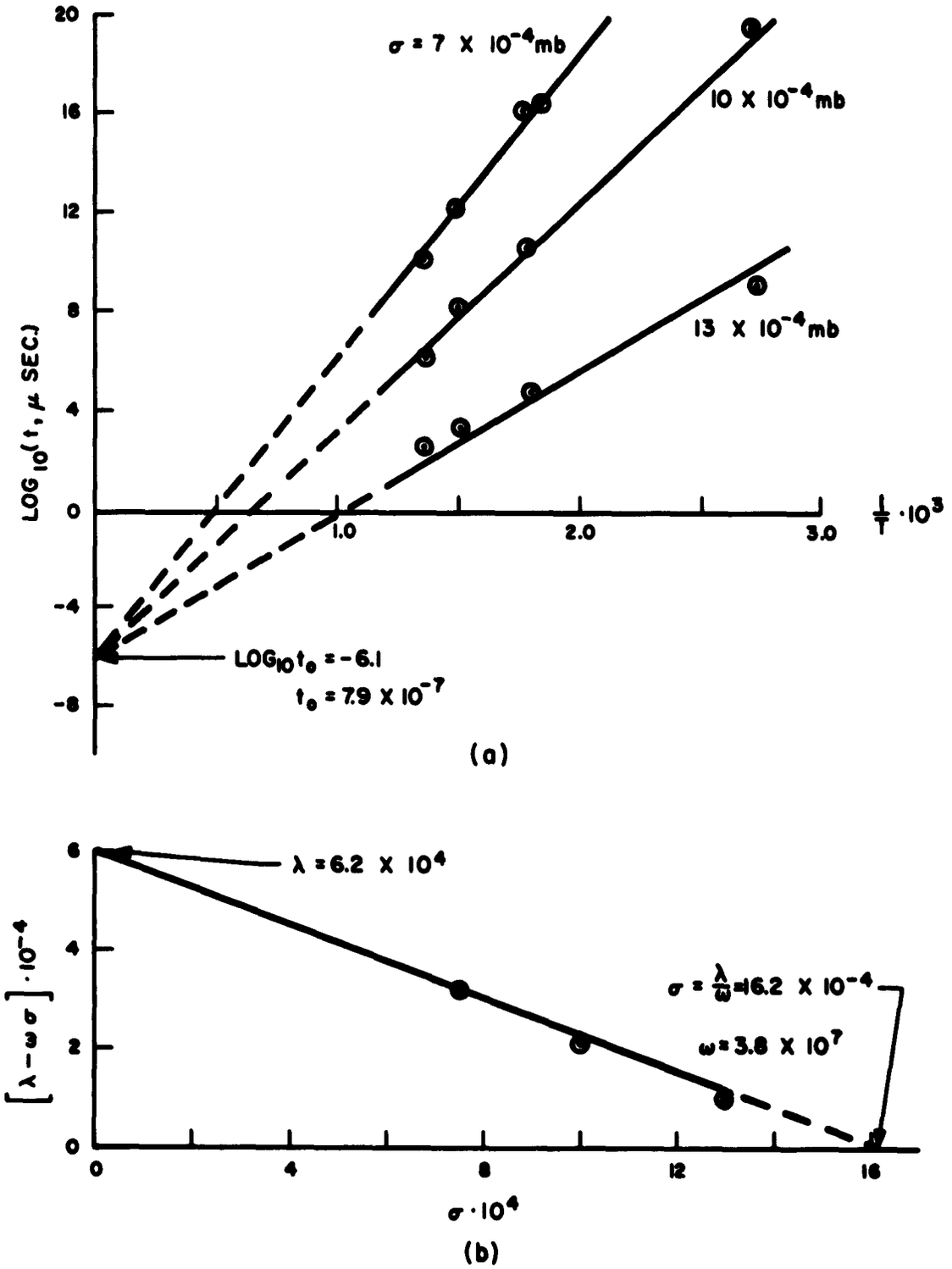

Figure 7. Strength-time-temperature behavior of aluminum (References 22 and 24) (a) Dependence of time to fracture on the absolute temperature (b) Dependence of $\lambda - \omega\sigma$ on σ.

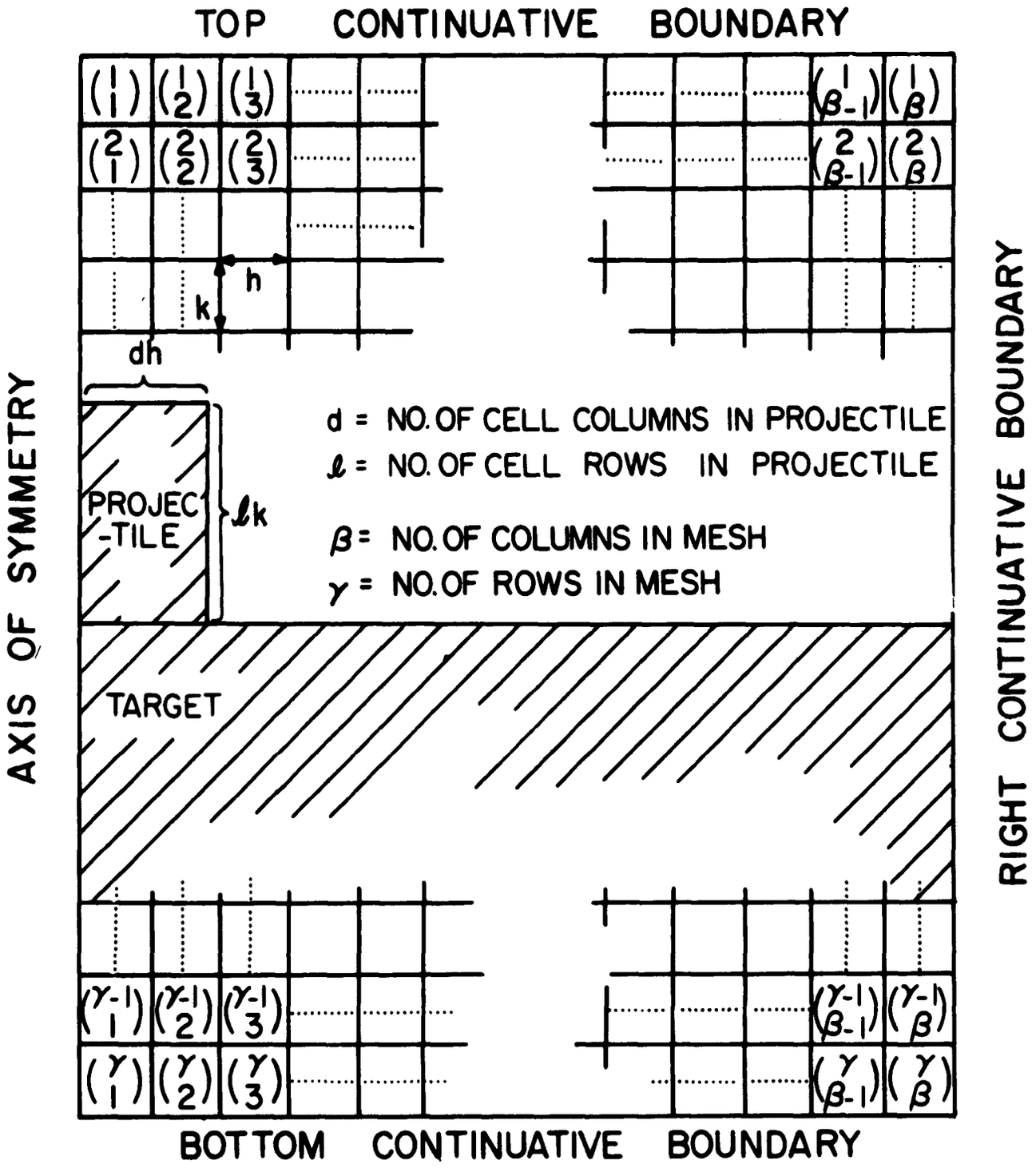

Figure 8. Rectangular mesh superimposed on the projectile-target configuration at instant of impact (t = 0).

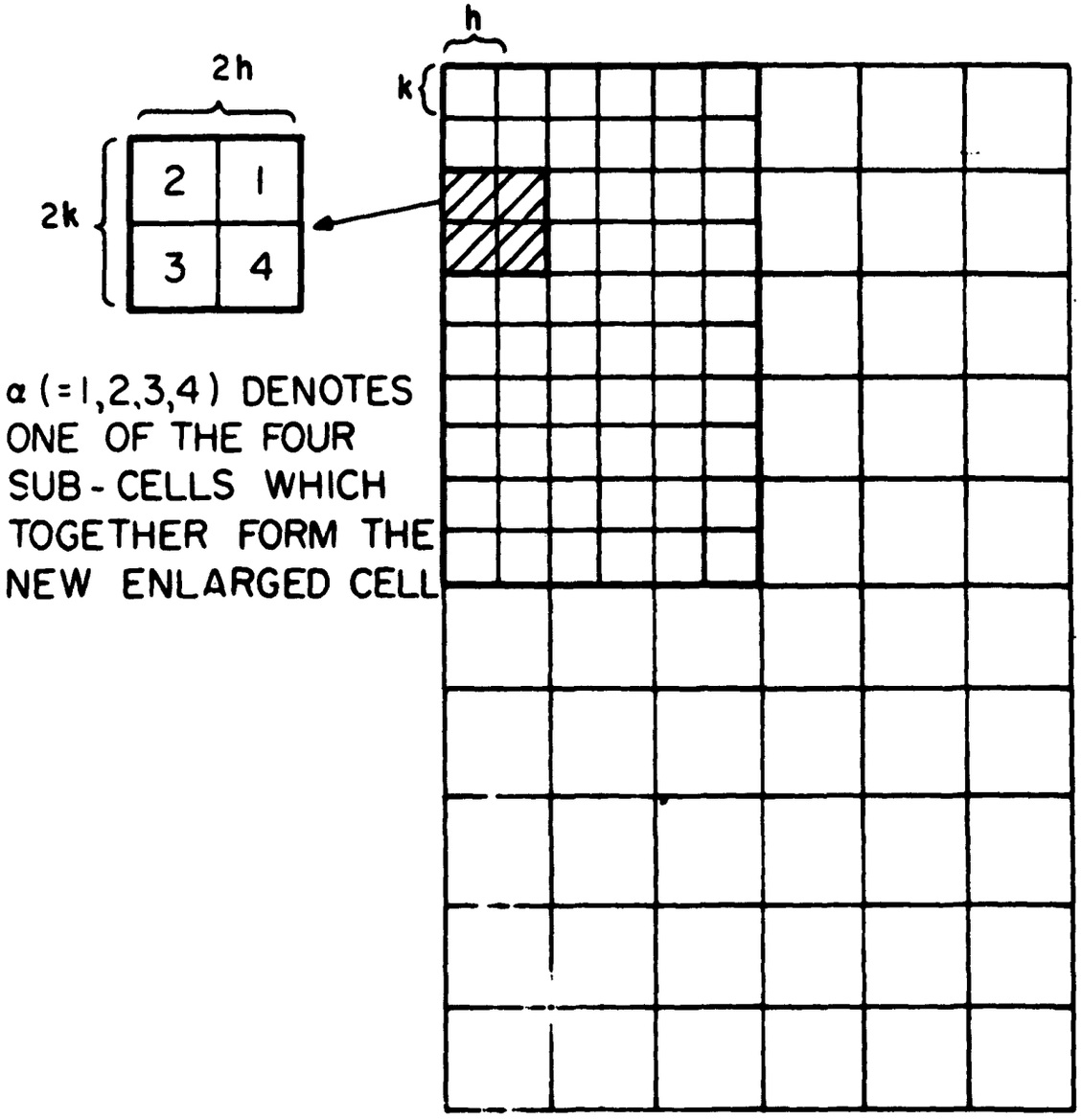

Figure 9. Schematic representation of the repartitioning in which the mesh area is increased four-fold.

INITIAL DISTRIBUTION

2	Wpns Sys Eval Gp
1	Hq USAF (AFTAC)
1	Hq USAF (AFCIN-3K2)
2	Hq USAF (AFRDC)
1	Hq USAF (AFRAE-E)
1	Hq USAF (AFTST-EL/CS)
1	Hq USAF (AFRST-PM/ME)
1	AFSC (SCRWA)
1	AFSC (SCTA)
2	BSD (AFSC)
1	ASD (ASAPRL)
1	ASD (ASRMDS)
3	ASD (ASAD-Lib)
1	ASD (ASRNGW)
2	SSD
1	OOAMA (OOYD)
2	AFSWC (Tech Info Div)
1	AFCRL (CRQST-2)
2	AFOSR
3	AFOSR (SRHP)
1	AFOSR (Univ of Utah)
1	TAC (TPL-RQD-M)
2	ARO (Scientific Info Br)
2	OAR (RROSA)
1	White Sands Msl Range (ORDBS-OM-W)
3	AMC (MCR)
2	Picatinny Arsenal (ORDBB-TK)
4	Aberdeen Proving Ground
1	Redstone Scientific Info Ctr
1	Frankford Arsenal (Lib)
1	Frankford (Pitman-Dunn Lab)
2	Springfield Armory (R&D Div)
2	Watervliet Arsenal (ORDBR-R)
2	Watertown Arsenal
1	Rock Island Arsenal
1	Engr Rsch & Dev Lab (Tech Support Br)
1	USCONARC (Spc Wpns Div)
2	U. S. Army Rsch Office
4	Bu of Nav Wpns (R-12)
4	Bu of Nav Wpns (RM)
1	Nav Rsch Lab
2	Naval Ordnance Test Station
2	Naval Ordnance Test Station (Tech Lib)
2	Naval Ordnance Lab (Tech Lib)
2	Naval Wpns Lab (Tech Lib)
1	USAF Proj RAND
1	NASA
4	NASA (Langley Rsch Ctr)
4	NASA (Ames Rsch Ctr)
1	Marshall Space Flight Ctr (M-AERO-TS)
1	Marshall Space Flight Ctr (Advanced Rsch Proj Lab)
1	Advanced Rsch Projects Agcy
1	Defense Rsch and Engineering (Tech Lib)
2	Defense Rsch and Engineering
1	Armour Rsch Foundation (Def Rsch)
3	Lewis Rsch Ctr
1	Univ of Chicago (Institute for Air Wpns)
2	The Franklin Institute of the State of Penn (Tech Lib)
1	Calif Institute of Technology (Jet Propulsion Lab)
2	Johns Hopkins University (Applied Rsch Lab)
30	ASTIA (TIPCR)
	APGC
2	ASQR
2	PGAPI
3	PGEH
2	PGWR
20	PGWRT
2	PGW

Air Proving Ground Center, Eglin Air Force Base, Florida
Rpt No. APGC-TDR-62-74. SOLUTION OF VISCO-PLASTIC EQUATIONS FOR AXISYMMETRIC HYPERVELOCITY IMPACT, Second Summary Report 3 November 1961 - 2 November 1962. Final report, December 196
91p. incl illus. tables, 36 refs. Unclassified Report

The dynamic response of a metallic body when impacted by a hypervelocity projectile is a complicated phenomenon involving the introduction of damage mechanisms which are not completely understood, even when independently operative. In Part I of this report, tentative phenomenological relations are proposed for the hypervelocity impact regime. They include (a) the flow resistance coefficient (which is of fundamental importance in the visco-plastic model for high speed impact), (b) the equation of state for both compressive and rarefaction regions of the metal, and (c) a fracture criterion for high intensity tri-axial stress distributions of extremely short duration. In Part II of the report a step-by-step description of a computational procedure is presented for the solution of the visco-plastic equations governing the axisymmetric hypervelocity impact situation. The procedure incorporates the above phenomenological relations which are necessary for a realistic description of the penetration and cratering processes. Finally, a brief resume is given of the considerations that were involved in developing PICWICK, an IBM 7090 computer program for carrying out the complex and lengthy computational procedure. This unique program is a basic tool in the development of a more complete theoretical understanding of the hypervelocity impact phenomenon.

1. Hypervelocity projectiles
2. Impact shock
3. Particles
4. PICWICK
I. OAR Project No. 9860
II. Contract AF 08(635)-1713
III. General Electric Company, King of Prussia, Pa
IV. Rissy, T. D.
V. In ASTIA collection

Air Proving Ground Center, Eglin Air Force Base, Florida
Rpt No. APGC-TDR-62-74. SOLUTION OF VISCO-PLASTIC EQUATIONS FOR AXISYMMETRIC HYPERVELOCITY IMPACT, Second Summary Report 3 November 1961 - 2 November 1962. Final report, December 196
91p. incl illus. tables, 36 refs. Unclassified Report

The dynamic response of a metallic body when impacted by a hypervelocity projectile is a complicated phenomenon involving the introduction of damage mechanisms which are not completely understood, even when independently operative. In Part I of this report, tentative phenomenological relations are proposed for the hypervelocity impact regime. They include (a) the flow resistance coefficient (which is of fundamental importance in the visco-plastic model for high speed impact), (b) the equation of state for both compressive and rarefaction regions of the metal, and (c) a fracture criterion for high intensity tri-axial stress distributions of extremely short duration. In Part II of the report a step-by-step description of a computational procedure is presented for the solution of the visco-plastic equations governing the axisymmetric hypervelocity impact situation. The procedure incorporates the above phenomenological relations which are necessary for a realistic description of the penetration and cratering processes. Finally, a brief resume is given of the considerations that were involved in developing PICWICK, an IBM 7090 computer program for carrying out the complex and lengthy computational procedure. This unique program is a basic tool in the development of a more complete theoretical understanding of the hypervelocity impact phenomenon.

1. Hypervelocity projectiles
2. Impact shock
3. Particles
4. PICWICK
I. OAR Project No. 9860
II. Contract AF 08(635)-1713
III. General Electric Company, King of Prussia, Pa
IV. Rissy, T. D.
V. In ASTIA collection

Air Proving Ground Center, Eglin Air Force Base, Florida
Rpt No. APGC-TDR-62-74. SOLUTION OF VISCO-PLASTIC EQUATIONS FOR AXISYMMETRIC HYPERVELOCITY IMPACT, Second Summary Report 3 November 1961 - 2 November 1962. Final report, December 196
91p. incl illus. tables, 36 refs. Unclassified Report

The dynamic response of a metallic body when impacted by a hypervelocity projectile is a complicated phenomenon involving the introduction of damage mechanisms which are not completely understood, even when independently operative. In Part I of this report, tentative phenomenological relations are proposed for the hypervelocity impact regime. They include (a) the flow resistance coefficient (which is of fundamental importance in the visco-plastic model for high speed impact), (b) the equation of state for both compressive and rarefaction regions of the metal, and (c) a fracture criterion for high intensity tri-axial stress distributions of extremely short duration. In Part II of the report a step-by-step description of a computational procedure is presented for the solution of the visco-plastic equations governing the axisymmetric hypervelocity impact situation. The procedure incorporates the above phenomenological relations which are necessary for a realistic description of the penetration and cratering processes. Finally, a brief resume is given of the considerations that were involved in developing PICWICK, an IBM 7090 computer program for carrying out the complex and lengthy computational procedure. This unique program is a basic tool in the development of a more complete theoretical understanding of the hypervelocity impact phenomenon.

1. Hypervelocity projectiles
2. Impact shock
3. Particles
4. PICWICK
I. OAR Project No. 9860
II. Contract AF 08(635)-1713
III. General Electric Company, King of Prussia, Pa
IV. Rissy, T. D.
V. In ASTIA collection

Air Proving Ground Center, Eglin Air Force Base, Florida
Rpt No. APGC-TDR-62-74. SOLUTION OF VISCO-PLASTIC EQUATIONS FOR AXISYMMETRIC HYPERVELOCITY IMPACT, Second Summary Report 3 November 1961 - 2 November 1962. Final report, December 196
91p. incl illus. tables, 36 refs. Unclassified Report

The dynamic response of a metallic body when impacted by a hypervelocity projectile is a complicated phenomenon involving the introduction of damage mechanisms which are not completely understood, even when independently operative. In Part I of this report, tentative phenomenological relations are proposed for the hypervelocity impact regime. They include (a) the flow resistance coefficient (which is of fundamental importance in the visco-plastic model for high speed impact), (b) the equation of state for both compressive and rarefaction regions of the metal, and (c) a fracture criterion for high intensity tri-axial stress distributions of extremely short duration. In Part II of the report a step-by-step description of a computational procedure is presented for the solution of the visco-plastic equations governing the axisymmetric hypervelocity impact situation. The procedure incorporates the above phenomenological relations which are necessary for a realistic description of the penetration and cratering processes. Finally, a brief resume is given of the considerations that were involved in developing PICWICK, an IBM 7090 computer program for carrying out the complex and lengthy computational procedure. This unique program is a basic tool in the development of a more complete theoretical understanding of the hypervelocity impact phenomenon.

1. Hypervelocity projectiles
2. Impact shock
3. Particles
4. PICWICK
I. OAR Project No. 9860
II. Contract AF 08(635)-1713
III. General Electric Company, King of Prussia, Pa
IV. Rissy, T. D.
V. In ASTIA collection

Air Proving Ground Center, Eglin Air Force Base, Florida
Rpt No. APGC-TDR-62-74. SOLUTION OF VISCO-PLASTIC EQUATIONS FOR AXISYMMETRIC HYPERVELOCITY IMPACT, Second Summary Report 3 November 1961 - 2 November 1962. Final report, December 1962 91p. incl illus. tables, 36 refs. Unclassified Report

The dynamic response of a metallic body when impacted by a hypervelocity projectile is a complicated phenomenon involving the introduction of damage mechanisms which are not completely understood, even when independently operative. In Part I of this report, tentative phenomenological relations are proposed for the hypervelocity impact regime. They include (a) the flow resistance coefficient (which is of fundamental importance in the visco-plastic model for high speed impact), (b) the equation of state for both compressive and rarefaction regions of the metal, and (c) a fracture criterion for high intensity tri-axial stress distributions of extremely short duration. In Part II of the report a step-by-step description of a computational procedure is presented for the solution of the visco-plastic equations governing the axisymmetric hypervelocity impact situation. The procedure incorporates the above phenomenological relations which are necessary for a realistic description of the penetration and cratering processes. Finally, a brief resume is given of the considerations that were involved in developing PICWICK, an IBM 7090 computer program for carrying out the complex and lengthy computational procedure. This unique program is a basic tool in the development of a more complete theoretical understanding of the hypervelocity impact phenomenon.

1. Hypervelocity projectiles
2. Impact shock
3. Particles
4. PICWICK

I. OAR Project No. 9860
II. Contract AF 08(635)-1713
III. General Electric Company, King of Prussia, Pa
IV. Riney, T. D.
V. In ASTIA collection

Air Proving Ground Center, Eglin Air Force Base, Florida
Rpt No. APGC-TDR-62-74. SOLUTION OF VISCO-PLASTIC EQUATIONS FOR AXISYMMETRIC HYPERVELOCITY IMPACT, Second Summary Report 3 November 1961 - 2 November 1962. Final report, December 1962 91p. incl illus. tables, 36 refs. Unclassified Report

The dynamic response of a metallic body when impacted by a hypervelocity projectile is a complicated phenomenon involving the introduction of damage mechanisms which are not completely understood, even when independently operative. In Part I of this report, tentative phenomenological relations are proposed for the hypervelocity impact regime. They include (a) the flow resistance coefficient (which is of fundamental importance in the visco-plastic model for high speed impact), (b) the equation of state for both compressive and rarefaction regions of the metal, and (c) a fracture criterion for high intensity tri-axial stress distributions of extremely short duration. In Part II of the report a step-by-step description of a computational procedure is presented for the solution of the visco-plastic equations governing the axisymmetric hypervelocity impact situation. The procedure incorporates the above phenomenological relations which are necessary for a realistic description of the penetration and cratering processes. Finally, a brief resume is given of the considerations that were involved in developing PICWICK, an IBM 7090 computer program for carrying out the complex and lengthy computational procedure. This unique program is a basic tool in the development of a more complete theoretical understanding of the hypervelocity impact phenomenon.

1. Hypervelocity projectiles
2. Impact shock
3. Particles
4. PICWICK

I. OAR Project No. 9860
II. Contract AF 08(635)-1713
III. General Electric Company, King of Prussia, Pa
IV. Riney, T. D.
V. In ASTIA collection

Air Proving Ground Center, Eglin Air Force Base, Florida
Rpt No. APGC-TDR-62-74. SOLUTION OF VISCO-PLASTIC EQUATIONS FOR AXISYMMETRIC HYPERVELOCITY IMPACT, Second Summary Report 3 November 1961 - 2 November 1962. Final report, December 1962 91p. incl illus. tables, 36 refs. Unclassified Report

The dynamic response of a metallic body when impacted by a hypervelocity projectile is a complicated phenomenon involving the introduction of damage mechanisms which are not completely understood, even when independently operative. In Part I of this report, tentative phenomenological relations are proposed for the hypervelocity impact regime. They include (a) the flow resistance coefficient (which is of fundamental importance in the visco-plastic model for high speed impact), (b) the equation of state for both compressive and rarefaction regions of the metal, and (c) a fracture criterion for high intensity tri-axial stress distributions of extremely short duration. In Part II of the report a step-by-step description of a computational procedure is presented for the solution of the visco-plastic equations governing the axisymmetric hypervelocity impact situation. The procedure incorporates the above phenomenological relations which are necessary for a realistic description of the penetration and cratering processes. Finally, a brief resume is given of the considerations that were involved in developing PICWICK, an IBM 7090 computer program for carrying out the complex and lengthy computational procedure. This unique program is a basic tool in the development of a more complete theoretical understanding of the hypervelocity impact phenomenon.

1. Hypervelocity projectiles
2. Impact shock
3. Particles
4. PICWICK

I. OAR Project No. 9860
II. Contract AF 08(635)-1713
III. General Electric Company, King of Prussia, Pa
IV. Riney, T. D.
V. In ASTIA collection

Air Proving Ground Center, Eglin Air Force Base, Florida
Rpt No. APGC-TDR-62-74. SOLUTION OF VISCO-PLASTIC EQUATIONS FOR AXISYMMETRIC HYPERVELOCITY IMPACT, Second Summary Report 3 November 1961 - 2 November 1962. Final report, December 1962 91p. incl illus. tables, 36 refs. Unclassified Report

The dynamic response of a metallic body when impacted by a hypervelocity projectile is a complicated phenomenon involving the introduction of damage mechanisms which are not completely understood, even when independently operative. In Part I of this report, tentative phenomenological relations are proposed for the hypervelocity impact regime. They include (a) the flow resistance coefficient (which is of fundamental importance in the visco-plastic model for high speed impact), (b) the equation of state for both compressive and rarefaction regions of the metal, and (c) a fracture criterion for high intensity tri-axial stress distributions of extremely short duration. In Part II of the report a step-by-step description of a computational procedure is presented for the solution of the visco-plastic equations governing the axisymmetric hypervelocity impact situation. The procedure incorporates the above phenomenological relations which are necessary for a realistic description of the penetration and cratering processes. Finally, a brief resume is given of the considerations that were involved in developing PICWICK, an IBM 7090 computer program for carrying out the complex and lengthy computational procedure. This unique program is a basic tool in the development of a more complete theoretical understanding of the hypervelocity impact phenomenon.

1. Hypervelocity projectiles
2. Impact shock
3. Particles
4. PICWICK

I. OAR Project No. 9860
II. Contract AF 08(635)-1713
III. General Electric Company, King of Prussia, Pa
IV. Riney, T. D.
V. In ASTIA collection